Geo-information Science and Remote Sensing

Thesis Report GIRS-2025-22

FISH HABITAT MAPPING USING LOCAL KNOWLEDGE, UAV, AND PLANETSCOPE IMAGERY

A Case Study on Humpback Mahseer (Tor remadevii) in the Cauvery River

Francesca Drăguț

April 8, 2025

WAGENINGEN
UNIVERSITY & RESEARCH

Fish Habitat Mapping Using Local Knowledge, UAV, and PlanetScope Imagery

A case study on Humpback Mahseer (Tor remadevii) in the Cauvery River

Francesca Drăguț

Registration number 1375512

Supervisors:

Arno Timmer
Harm Bartholomeus

Collaborator

Naren Sreenivasan
(Wildlife Association of South India)

A thesis submitted in partial fulfilment of the degree of Master of Science
at Wageningen University and Research Centre, The Netherlands.

Thesis code number: GIRS-2025-22
Wageningen University and Research Centre
Laboratory of Geo-Information Science and Remote Sensing

April 8, 2025
Wageningen, The Netherlands

Statements

Permission

The field aspect of the project was conducted in collaboration with the Wildlife Association of South India (WASI), a registered non-governmental agency with headquarters in Bengaluru City. Permission to conduct field work was secured by WASI via document: PCCF (WL)/E2/CR-78/2017-18.

Use of generative artificial intelligence

Generative artificial intelligence (GenAI) was mainly used for creating charts and adjusting visualisation parameters in R. GenAI was also used in issues related to LaTeX code, such as citation formatting, mathematical equations, and formatting figures with multiple panels. It was also used for code debugging. However, the responses provided by GenAI were critically judged before being implemented.

Photography credits

All photographs featured in this report, taken within the study area, are the property of the research team, including the author, Naren Sreenivasan, and Anisha Gogoi. These images are available for use and distribution upon request from the author or the team members.

Acknowledgements

I am incredibly grateful to Naren Sreenivasan, and the Wildlife Association of South India, for hosting me in India and giving me the chance to experience the Cauvery Wildlife Sanctuary, an area accessible to very few people. I am thankful for the knowledge and wisdom I gained from Naren, the research team from India, and the journey itself. I am immensely thankful to my supervisors, who encouraged me to take on this journey, and for their endless support throughout the entire thesis process. My gratitude also goes to my colleagues and friends - Lorena and Yannick -, who helped me with point annotation and support.

Abstract

The critically endangered Humpback Mahseer (Tor remadevii) fish species, endemic to the Cauvery River in South India, requires habitat maps to support species reintroduction, an effort coordinated by the Wildlife Association of South India (WASI). To localize reintroduction areas, an automated and scalable method is needed to derive habitat maps. WASI acquired a UAV image of a 3km river stretch, on which 8 habitats were identified: pool, shallow, rapid, pebble beach, rock, sand, riparian vegetation, and scrub jungle. Although UAV images are effective in classifying river habitat, they are costly and inefficient to acquire in multiple areas. This study explored the use of PlanetScope (PS) imagery and textures (homogeneity, entropy, variance) for habitat classification using local knowledge to derive training samples from UAV. Three Random Forest models were trained on one river stretch and tested on two others, using: (1) all PS bands and textures, (2) only textures on all PS bands, (3) red and near-infrared (NIR) bands and textures. Results show that an iterative process including local knowledge is efficient in deriving training samples from UAV imagery. On average, the model trained only on textures performed best in all areas: 0.56 recall and precision, and 0.89 accuracy. Although the model trained on textures and bands performed better for some habitats of the test areas (e.g. pebble beach, rock), it performed poorly in others (e.g. rapids, with some metrics reaching 0).This study shows that combining UAV, local knowledge, and high-resolution satellite imagery is effective in habitat mapping. While previous studies used textures in combination with other predictors, this study showed that using textures alone is a feasible and more generalizable alternative. This approach will enable WASI experts to up-scale habitat mapping across the Cauvery River, supporting data-driven conservation and species reintroduction efforts.

Contents

Chapter 1

Introduction

1.1 Background

Humpback Mahseer (*Tor remadevii*) (**Figure 1.1**) is a highly important fish species, endemic to the Cauvery River Basin in South India (**Pinder et al., 2018b**). Humpback Mahseers belong to the megafauna, with some specimens weighing more than 50kg (**Pinder et al., 2018b**, **Sreenivasan, 2025a**). Although research has been done in the past few years, Humpback Mahseers are to this day the only critically endangered mahseer species (**IUCN, 2024**, **Pinder et al., 2020**).

Figure 1.1. Humpback Mahseer. Source: **Pinder et al. (2018b)**.

Humpback Mahseers can be found in several areas of the Cauvery River Basin. However, a particularly important area for them is the Cauvery Wildlife Sanctuary (CWS). The CWS is a protected area, under the management of the Widlife Association of South India (WASI). In 1976, WASI established catch-and-release (C&R) angling camps in the Cauvery Wildlife Sanctuary (CWS), their success being followed by other organisations as well (**Gupta, 2015**). C&R angling is historically and culturally relevant practice in India (**Hamilton, 1822**), and has proven effective in tracking fish species.

In their study, **Pinder et al. (2015a)** collected C&R data from the Galibore Nature Camp, one of the protected former angling camps in the CWS. Using this data, it was observed that in 1980s a new Mahseer phenotype has been introduced in the Cauvery River. In their study, **Pinder**

et al. (2015b) argue that this new blue-finned Mahseer phenotype gradually appropriated the habitats of the Humpback Mahseers. However, the causes of the decline of the Humpback Mahseer population are multiple and complex, and the phenomenon cannot be entirely blamed on the blue-finned phenotype (Sreenivasan, 2024).

Indeed, a dramatic population shift was observed in 2004, as shown in the study conducted by Pinder et al. (2015a). In 2004 a high decrease in Humpback Mahseer populations happened simultaneously with a high increase in blue-finned Mahseer population. However, this does not imply that blue-finned Mahseers are invasive, because the shift is correlated with a prolonged drought which persisted from 2001 to 2004 in South India (Venot et al., 2010, Sreenivasan, 2025a). With appropriate conditions, blue-finned and Humpback Mahseers would choose different spawning and feeding places. Therefore, the root cause for Humpback Mahseer population decline is the degradation of habitat quality and availability, which have several causes. Among them, destructive dynamite fishing, lack of river protection status, and river damming are the most significant. For instance, a dam project threatens to submerge a large part of the Cauvery Wildlife Sanctuary (detailed in Appendix A).

WASI is actively working on establishing a baseline conservation action plan. This plan aims to find reintroduction areas for Humpback Mahseers in the Cauvery River and to prevent river damming in the area. They do this by collaborating with key government agencies. The Karnataka Forest Department is one such agency, with which WASI collaborates on establishing brood stock from the remaining populations of Humpback Mahseer (Sreenivasan, 2024). However, to repopulate different areas of the Cauvery River with the established brood stock, a geospatial study is needed, including habitat and behavioural trends. To obtain this, fish movement data needs to be accompanied by habitat maps, to derive habitat preferences and population trends.

According to the experts at WASI and previous studies (Pinder et al., 2018a), Humpback Mahseer habitat maps in Cauvery River are currently lacking. To address this issue, WASI acquired a UAV orthophoto of an area within the Cauvery Wildlife Sanctuary. Moreover, field experts at WASI have identified a number of habitat types specific to Humpback Mahseers, along with their ecological properties. However, this knowledge needs to be aggregated into a method capable to automatically map habitats from remote sensing imagery.

Humpback Mahseer habitat maps would help WASI in quickly identifying potential repopulation areas. In addition, they would help justify the need to declare river stretches as conservation areas to government agencies (Sreenivasan, 2024). This is valuable because there is currently no legal conservation enforcement. The only protection for Humpback Mahseer comes from community social enforcement (Nautiyal, 2014).

Given the high habitat heterogeneity of the area, and the increasing need to declare protected areas, the habitat identification method needs to be generalizable and scalable, as river transects vary in habitat composition. The goal of this research is to develop an automatic and generalizable Random Forest model for mapping areas within the Cauvery River, using local knowledge as baseline information for training data and analysis.

1.2 Related work

In their global synthesis on habitat modelling in fish ecology, Wegscheider et al. (2020) identified two main mapping techniques. The first one is based on manual field surveys, using descriptive criteria and thresholds for physical and hydraulic parameters. The second one is automated classification, using remote sensing and modelling. Even though field measurements are more reliable, remote sensing is useful in isolated areas (Giroux et al., 2022). There are several classification techniques, based on either machine learning or deep learning. Machine learning algorithms are more feasible in remote environments, requiring less training data than deep learning models, and generalizing well in new contexts (Pichler and Hartig, 2023). For classification tasks, machine learning can be generally divided into unsupervised, supervised, and rule-based algorithms (Hurbean et al., 2021). Unsupervised algorithms, or self-organizing maps, do not require training data for classification. Unsupervised algorithms, such as K-Means clustering, and Isodata, cluster data statistically, based on spectral similarity, without prior knowledge on the classes (Lauer and Aswani, 2008). However, the derived classes need to be labelled post-classification. Studies show good results in unsupervised habitat mapping (Mohamed et al., 2022, Lauer and Aswani, 2008). However, to derive a classification method specifically for Humpback Mahseers, adding prior knowledge on the habitats might be useful.

Classification can further be divided into pixel-based and object-based. Pixel-based approaches directly classify each pixel, while object-based approaches focus on first segmenting the image into objects and then labelling them. Pixel-based approaches have been used in several habitat mapping studies (Lauer and Aswani, 2008, Tan et al., 2023, Zhang and Fryirs, 2024). On the other hand, object-based methods are more frequently used in landform classification, with lower heterogeneity levels and more available terrain data (Wahidin et al., 2015, Blaschke, 2010). In their study, Stone et al. (2024) compared pixel-based and object-based techniques in mapping coral reefs from UAV imagery. According to their results, the pixel-based approach had higher accuracy. They explain this could be due to difficulty in spectral separation between *coral* and *rubble/rock* classes in a highly heterogeneous and fine-scale context, which is comparable to the current study area.

Pixel-based supervised classification uses training data as prior knowledge, learning class properties based on statistics of significant samples of the predictor features (Kotsiantis et al., 2007). In their study, Berhane et al. (2018) compared decision trees, Random Forest, and rule-based classification in wetland mapping in WorldView-2 images of the Selenga River Delta in Siberia, Russia. According to the results, RF outperformed the other methods. Moreover, RF tends to produce better results when fewer training samples are available, showing a fast, simple and optimised procedure (Zagajewski et al., 2024).

Fish habitats are placed within the margins of the river bed (Wheaton et al., 2015) and partially correspond to geomorphic units, placed on the meso-scale (10^0 to 10^2m) (Belletti et al., 2017). To map habitats on the meso-scale from remote sensing products, high-resolution imagery needs to be used. Most studies with similar contexts use drone imagery (Giroux et al., 2022, Stone et al., 2024, Woodget et al., 2017, Fallati et al., 2020, Ventura et al., 2018). Others use WorldView-2 (Berhane et al., 2018, Tang et al., 2016, Halder et al., 2024). Less studied for habitat mapping, but having high potential is PlanetScope data (An et al., 2023, Zagajewski et al., 2024), with a spatial resolution of 3m.

High quality data is a requirement for both training data and predictors. Several studies exploring aquatic habitat classification included gray-level co-ocurrence matrix (GLCM) textures as predictors (Giroux et al., 2022, Zhang and Fryirs, 2024, Hall-Beyer, 2017, Berhane et al., 2018). Apart from GLCM textures, local spatial statistics - such as Local Moran's I, Getis-Ord Local Gi and Local Geary's C - were useful in benthic habitat mapping (Collin et al., 2011).

In their study, Giroux et al. (2022) analyzed salmon habitats in Canadian rivers. The study used UAV imagery, and textural features derived from UAV. The textural features they used include homogeneity, contrast, and mean intensity. They used supervised classification, to separate the dry and submerged river areas from the riparian vegetation. To assess accuracy, they generated random points within the training samples, which were omitted from training. The riparian vegetation was masked out, and dry and submerged areas underwent texture analysis, object-based image analysis, and supervised classification. Textures computed on the UAV image bands were used in image segmentation. The obtained segments were then classified using supervised classification, based on training data annotated on the UAV image.

Different texture predictor combinations have been previously used. In their study, Zhang and Fryirs (2024) used angular second moment on the green, red, and NIR bands, to determine river habitats. Adding indices as predictors, alongside textural features and the original bands can lead to accuracy improvements, as shown by Zhang et al. (2017). Indices like normalized difference vegetation index (NDVI), normalized difference water index (NDWI), and normalized difference soil index (NDSI), have been used by Berhane et al. (2018). The same study used a digital elevation model (DEM) and other DEM-derived hydrogeomorphic metrics (landscape position, surface depression, and distributary stream channels), increasing classification accuracy.

1.3 Research Gap

Even though there were multiple studies related to habitat mapping for different species or river systems, there is no previous study classifying Humpback Mahseer habitats. Moreover, most studies related to fish habitat classification used UAV imagery, which is not feasible financially and computationally when upscaling to multiple areas. An automated and scalable classification method is essential in creating habitat maps in the heterogeneous area of the Cauvery River. Moreover, precise habitat maps for Humpback Mahseers are important in supporting further research, such as deriving habitat preferences and population trends for Humpback Mahseers.

1.4 Proposed Solution

The approach is to derive training samples from UAV imagery and local knowledge, and to integrate them into a Random Forest algorithm using different predictor combinations based on PlanetScope data, each corresponding to a model. Accuracy assessment will be performed to decide which model is the most generalizable for multiple river transects.

1.5 Research Questions

To develop an automated and scalable model for Humpback Mahseer habitat classification in the Cauvery River using local knowledge, UAV and PlanetScope imagery, this study investigates:

1. How can local knowledge be used in creating training samples of Humpback Mahseer habitats on UAV imagery?
2. What predictors can be used in training Random Forest for Humpback Mahseer habitat mapping?
3. Which predictor choice produces the highest accuracy?

Chapter 2

Methods

2.1 Study area

The Cauvery Wildlife Sanctuary (CWS) is an area with rich biodiversity, situated in the Deccan plateau, between the Western and the Eastern Ghats (Figure 2.1). The Western Ghats is a high mountain range, with rainforest characteristics and 40% to 60% endemism, depending on the fish species (Sreenivasan, 2025a, Menon and Bawa, 1997). The Eastern Ghats is a lower mountain range, with scrub jungle characteristics (Sreenivasan, 2025a).

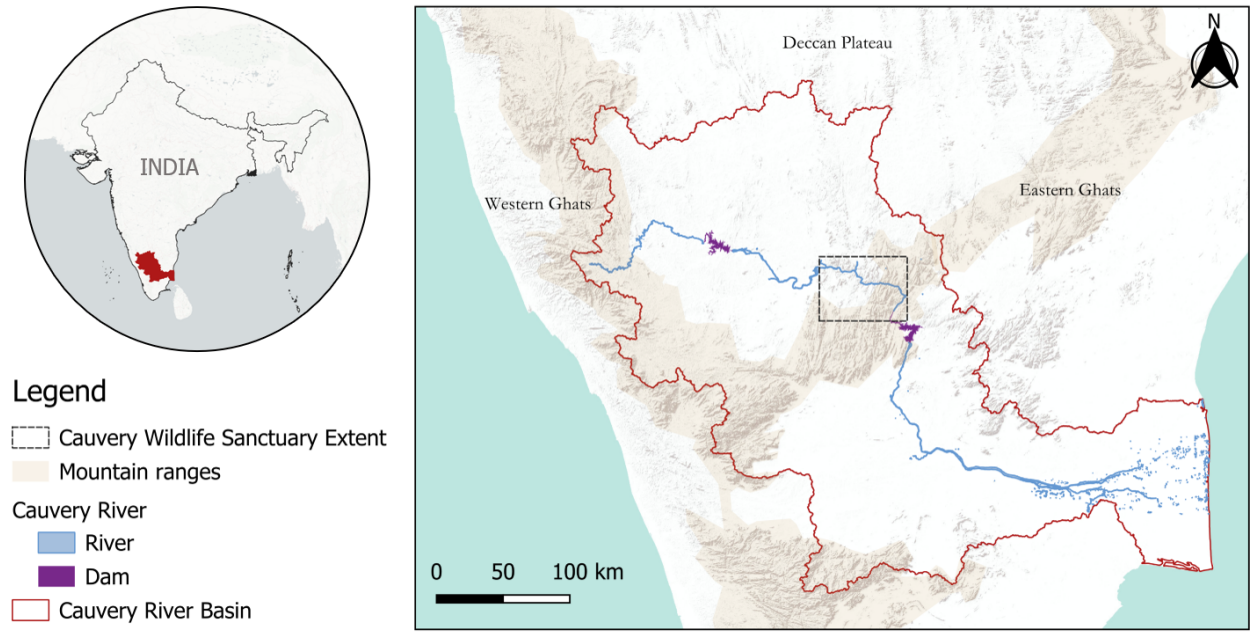

Figure 2.1. Geographic overview of the Cauvery Wildlife Sanctuary within the Cauvery River, showing the sanctuary extent, the main river channel, dams, and surrounding mountain ranges. The inset map provides an overview of the location of the study area within India.

The location of the CWS geographically makes it a meeting point for wildlife from both Western and Eastern Ghats, which find optimal habitat characteristics in the Cauvery River Valley (Sreenivasan, 2025a). Therefore, the CWS is home to a wide range of species of mammals, birds, reptile, and fish species.

From a river morphology perspective, the river elevation profile determines the river character, which in turn, determines the wildlife variety from a particular stretch (Sreenivasan, 2025a). The CWS is situated in the middle course, which is divided into three stretches (Figure 2.2). In their study, Sreenivasan and Mahesh (2021) described the three stretches of the middle course. The upper stretch (A) shows high stream braiding, with predominantly shallow water, while the lower one displays mainly slow flowing pools (stretch C). The middle stretch (B) shows traits of both the upper and lower courses. Galibore and Bheemeshwari are situated in stretch A, while Mekedatu is at the border between stretch A and B. The abrupt elevation change in stretch A determines high habitat heterogeneity, where a high variety of freshwater fish species find optimal conditions, including the Humpback Mahseer.

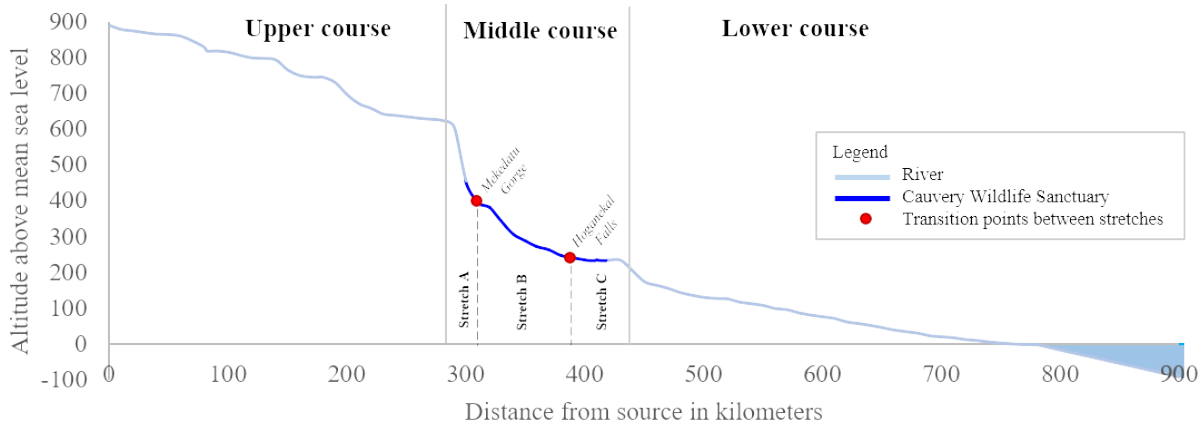

Figure 2.2. Elevation profile of the Cauvery River, along the upper, middle, and lower courses. Source: Naren Sreenivasan, Wildlife Association of South India.

2.1.1 River boundaries

During an interview with Naren Sreenivasan from 28.10.2024, it was identified that there is an ecological boundary of the river. This boundary is defined by the maximum water extent reached during the monsoon season and the riparian vegetation. The reduced water levels make the boundary less visible, but expose part of the river substrate. During the monsoon, increased water levels inundate the river banks, integrating them into the river substrate, where they are used by Humpback Mahseers. Therefore, the dry season is relevant in habitat mapping, as it exposes a large part of the river substrate which is used by fish during the monsoon (Zhang and Fryirs, 2024, Sreenivasan, 2024). In the same interview, 8 habitat types were identified within the river boundaries, discussed in Section 2.1.2.

2.1.2 Humpback Mahseer Habitats

The following habitats relevant to Humpback Mahseers are found in the river boundaries: **pool**, **shallow**, **rapid**, **pebble beach**, **rock**, **sand**, **riparian vegetation**, **scrub jungle** (Figure 2.3).

(a) Pool

(b) Shallow

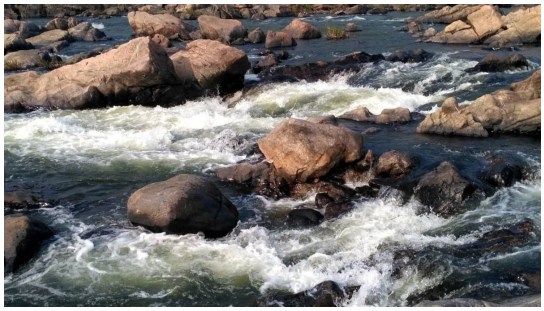

(c) Rapid

(d) Pebble beach

(e) Rock

(f) Sand

(g) Riparian vegetation

(h) Scrub jungle

Figure 2.3. Habitat types relevant for Humpback Mahseers within the ecological river boundaries.

Pools

Pools (Figure 2.3a) are deep, slow-flowing water bodies, which provide safe areas for Humpback Mahseers (Sreenivasan and Mahesh, 2021). They use pools especially when the water levels are low throughout the river. During low water levels, especially in April and May, water, food and oxygen are scarce. Therefore, fish stay in pools, which provide rather constant water levels, unlike rapids or shallow waters, which can be completely dry during droughts.

Shallows

Shallows are represented by slow-flowing water (in-channel) or still water (outside-channel) (Figure 2.3b). In-channel shallow waters are used as transition areas between pools and rapids. Outisde-channel pools consist of still shallow water. During dry season, they are disconnected from the main channel, being used as fish nurseries and refuge for juveniles. Compared to pools and rapids, shallows have higher temperature and lower velocity, promoting micro-vegetation growth, which makes them look greener, due to higher chlorophyll concentration.

Rapids

Rapids (Figure 2.3c) are characterised by fast water colliding with rocks. Due to oxygenation occurring when water hits rocks, rapids have lower temperatures. When water levels are low in the river, rapids do not provide enough water for the large size of the Humpback Mahseers. However, when water levels increase, water rapidly drops downstream, taking along high amounts of feed. Due to the rocky structure of the rapids, the feed is isolated, making rapids ideal for hunting and feeding.

Pebble beaches

Pebble beaches (Figure 2.3d) are essential refuge places for juvenile fish. The pebble beaches are usually located near rapids. Areas where pebble strips are present are likely to become inundated during monsoon, covered by shallow water. On larger pebble beaches, shrubs and vegetation can be present.

Rock

Rocks (Figure 2.3e) in the Cauvery River are composed of metamorphic granitic gneiss (Sreenivasan and Mahesh, 2021). They provide safe areas for Humpback Mahseers from predators, such as carps, eels and otters (Sreenivasan, 2024). Rock is also present on the river bank.

Sand

Sand bars (Figure 2.3f) are important spawning habitats. During monsoon, when sand bars become part of the substrate, female mahseers lay eggs in these areas. Some sand bars are placed under the canopy of the riparian belt, making their identification difficult from remotely sensed data.

Riparian vegetation belt

The riparian vegetation belt (Figure 2.3g) is represented by the deciduous evergreen forest, placed on the sides of the river bank and sometimes on the islands in the main channel. It represents an important food source for fish. Moreover, the roots of the riparian vegetation sustain the bank integrity during the monsoon, when the bank is flooded. During monsoon, fish use the intricate structure of vegetation for refuge. During dry season, only the riparian vegetation stays green. More detailed information on the ecology of the riparian belt is shown in Appendix B.

Scrub jungle

Scrub jungles (Figure 2.3h) consist of dry deciduous forest, representing the dominant forest type in the CWS (Sreenivasan and Mahesh, 2021). Scrub jungle is located beyond the riparian vegetation belt. The difference between riparian vegetation (foreground) and scrub jungle (background) can be seen in Figure 2.3g. During dry season, scrub jungle dries to a higher rate than the riparian vegetation, due to distance from the river. Scrub jungles have minor direct influence on the fish. They host almost the same variety of animals as the riparian belt. Therefore, scrub jungle also contributes to the overall health of the riverine ecosystem.

2.1.3 Fieldwork observations

Additional information about each study area and habitat transitions in the context of river dynamics were obtained during a field campaign organized with the Wildlife Association of South India (02-07.02.2025). The team consisted of the author, and local experts: Naren Sreenivasan, two local fisherman, and two zoology interns. The CWS has high habitat variability, making each zone unique in terms of habitat composition.

In **Galibore**, the predominant aquatic habitat is *pool*. The predominant land habitat is *pebble beach*, placed in the proximity of rapids. The canopy coverage of the riparian vegetation is low, making the area visible from remotely sensed imagery. The river bed is wide, with relatively flat terrain, surrounded by distant hills. In-field observations showed an additional habitat, composed of a mix of sand and rock (Figure 2.4a). In the proximity of outside-channel habitats, pebble beaches falsely look like they are covered in sand during dry season (Figure 2.4b). Due to the shallow static water, moss grows on the pebble when it is covered in water. When water evaporates during dry season, the dried moss looks like sand.

In **Bheemeshwari**, the river is more braided than in Galibore. Therefore, pools, shallows and rapids become intertwined. Pools are smaller and they transition into shallows and rapids more frequently than in Galibore. The canopy coverage of the riparian vegetation is high, which makes it difficult to classify some of the areas from remotely sensed imagery. The river bed is wide, but the area is surrounded by high hills, which are placed in the proximity of the river bank. In-field observations show a high amount of exposed rock within the main channel of the river (Figure 2.4c). According to local experts, exposed rocks within the river channel are likely to become rapids when water levels increase (Sreenivasan, 2025b).

Mekedatu is the narrowest point in the entire Cauvery River, having a canyon-like structure. The predominant habitat is rock (**Figure 2.4d**). Downstream of Mekedatu, the river begins to transition to the second stretch of the middle course, where habitat and species heterogeneity decrease. During dry season, water levels are particularly low in Mekedatu, with small and narrow pools. The topography becomes increasingly abrupt towards the south, with steep hills descending into the river bed, leaving minimal transition zones between the river bed and the hills.

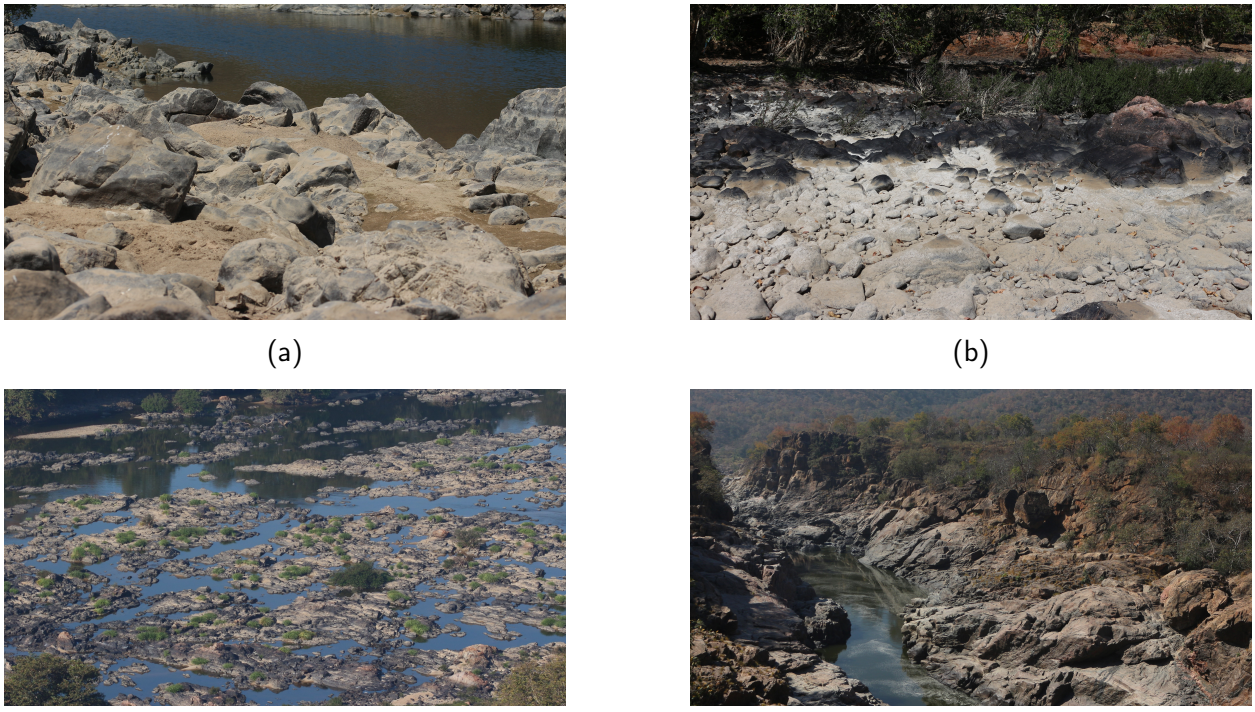

(a) (b)

(c) (d)

Figure 2.4. (a) Galibore: rock covered in sand; (b) Galibore: pebble covered in dry moss; (c) Bheemeshwari: exposed rock in the river; (d) Mekedatu: rock canyon.

2.2 Data

During a field campaign organised by WASI on 29.03.2024, a UAV orthophoto with 3cm resolution was acquired in the area surrounding the Galibore Natural Camp (Figure 2.5).

Figure 2.5. UAV image of the Galibore area.

The UAV image was used for creating training samples, which were later used to train a Random Forest (RF) algorithm on a PlanetScope (PS) image from the same date as the UAV image (Figure 2.6). The image was acquired with a PSB.SD sensor, with 3m resolution. Available bands are blue, green, red and near-infrared (NIR). The Galibore area was used for training, while Bheemeshwari and Mekedatu were test areas.

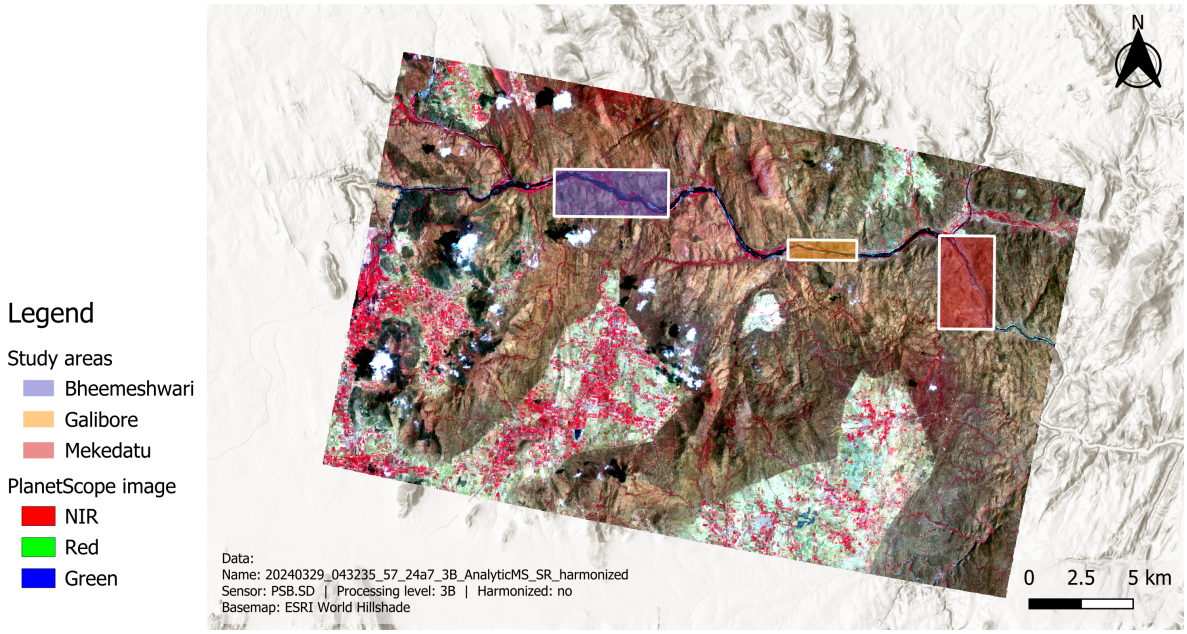

Figure 2.6. Study areas within the PlanetScope image extent. The areas shown on the map are Bheemeshwari, Galibore, and Mekedatu.

Appendix C provides detailed metadata and data management information for both existing and created datasets.

2.3 Image preprocessing

The preprocessing of PlanetScope imagery consisted of:

- Cloud and shadow correction
- Cropping the image to the study areas
- Determining and cropping the river bed boundaries for each study area

As part of data preparation, the PS image was masked using the *clear* band of the associated UDM2 data mask. This operation eliminated cloud cover, shadow, light and heavy haze from the image. The masked bands were also normalized in a range from 0 to 1. On visual inspection, the UAV and PS images were not perfectly aligned, and a freehand georeferencing tool[1] was used to correct this, by shifting the UAV image.

To establish the study areas, a new polygon layer was created. Polygons were manually drawn around the former fishing camps. Their extent was extracted, to obtain the rectangular areas seen in Figure 2.6. The study areas contain river stretches of: 3.5km (Galibore), 5.5km (Bheemeshwari), and 4.5km (Mekedatu). Using study areas with river stretches of 3-5km is relevant in the context of habitat heterogeneity. Habitat composition changes even in 1km river stretches. Study area sizes between 3 and 5 km are the ideal size for capturing local variability and deriving habitat composition specific to an area.

Another part of the image preprocessing consisted of extracting the river bed boundaries and cropping the study areas to those boundaries. The boundaries were extracted for several reasons.

Firstly, the water extent during dry season is significantly lower than during the monsoon. The habitats which correspond to land forms (sand, pebble beach, rock, riparian vegetation) and are only visible during dry season. During the monsoon, they are submerged and become part of the river bed, being used by Humpback Mahseers in different ways (see Section 2.1.2). The riparian vegetation belt represents an ecological border of the river during the monsoon. It is also relevant because most of the time, sand bars or pebble beaches lie underneath the canopy, which is not visible from remotely sensed imagery (Sreenivasan, 2025b).

Secondly, the river boundaries extraction was done for statistical reasons. Beyond the riparian vegetation belt, the landscape mostly contains scrub jungle, which rarely becomes submerged by water during the monsoon. Therefore, it is of little relevance to Humpback Mahseers (Sreenivasan and Mahesh, 2021). Without this boundary setting operation, further analyses and statistics would be skewed, showing disproportionately high scrub jungle occurrence.

[1] Freehand Raster Georeferencer Plugin in QGIS

To determine the month with maximum water extent, historical monthly outflow data between 1974 and 2012 from the Krishna Raja Sagara dam was used. The highest outflow month was determined to be August (Figure 2.7).

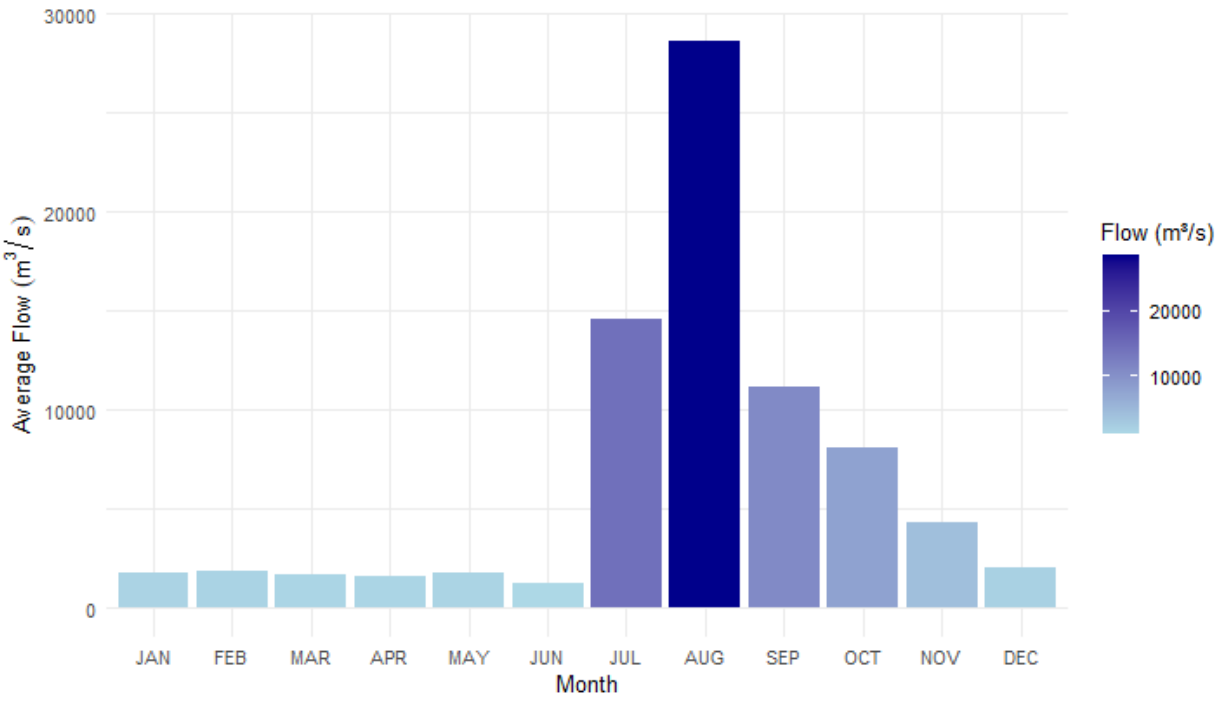

Figure 2.7. Average flow per month (1974 to 2012) from Krishna Raja Sagara Dam. August is the month with the highest flow.

Studies show that water can be extracted from optical data, using a normalized difference water index (Halder et al., 2024). However, this method is limited by cloud cover, specific to optical sensors (Portales-Julia et al., 2023). This is an issue because maximum water level is reached during monsoon, which has dense and almost permanent cloud cover. Radar data proved to be a feasible option in similar contexts (Ruzza et al., 2019). Therefore, all available Sentinel-1 VH images were retrieved for the month of August 2024 for the Cauvery Wildlife Sanctuary. The images were masked using a Shuttle Radar Topography Mission (SRTM) image in the same extent, where only values below 450 meters were considered as part of the river valley. The images were averaged, to obtain an overview of the water extent in August. The mean raster was cropped to each study area extent (Figure 2.6). For each study area, Otsu's algorithm was used to derive a threshold for separating *water* from *non-water*. Otsu's thresholding is a statistical method, efficient in binary segmentation tasks (Xu et al., 2011). The water mask was polygonized, and filtered to the largest contiguous area, to obtain the main river channel. However, in Mekedatu, because of the low amount of water, there were multiple polygons corresponding to the main river area, so the polygons were manually filtered.

Regarding the riparian vegetation belt, there are multiple ways to extract evergreen vegetation. Several studies indicate that using a normalised difference vegetation index (NDVI) is a simple and standardized way to assess the amount of vegetation in remote sensing (**Liu, 2017**, **Rouse Jr et al., 1974**). The NDVI was computed on all study areas using **Equation 2.1**.

$$\text{NDVI} = \frac{\rho_{\text{NIR}} - \rho_{\text{RED}}}{\rho_{\text{NIR}} + \rho_{\text{RED}}} \quad \text{, where} \tag{2.1}$$

ρ_{NIR} is the reflectance of the NIR band and
ρ_{RED} is the reflectance of the red band

For each study area, the maximum, mean (μ), and standard deviation (σ) of the NDVI were computed. A threshold using these values was computed for each area using **Equation 2.2**. The values above this threshold represent the upper end of the histogram distribution, where the greenest vegetation is found. Therefore, this threshold can be used to separate evergreen vegetation from other types of seasonal forests.

$$\text{threshold} = \max_{\text{NDVI}} - \mu_{\text{NDVI}} + \sigma_{\text{NDVI}} \tag{2.2}$$

For each study area, the binary water mask and the binary evergreen vegetation mask were summed, filtered for valid values, and polygonized. The area for each polygon was computed. The polygon with the maximum area was considered as the main river boundary, while the other ones were deleted. The main polygon was buffered on a distance of 50 meters, to account for any potential errors. Finally, holes within the polygons were filled.

2.4 Training sample creation

Using local knowledge in training data creation proved to be effective in riverine landscapes, where little conventional data is available (Wegscheider et al., 2024, Martin et al., 2012, Lauer and Aswani, 2008). Even though training data can be created automatically or semi-automatically (Pagels et al., 2024, Ierodiaconou et al., 2018, Janowski and Wróblewski, 2024), manual annotation was chosen to accommodate local knowledge. Therefore, the hypothesis is that manually derived UAV training samples can be used for supervised classification of fish habitats in PlanetScope imagery, despite the difference in resolution.

Since quality of the training samples is important in supervised classification (Millard and Richardson, 2015, Xia et al., 2015), training samples were obtained in three iterations. The first iteration was created during an interview with Naren Sreenivasan, where areas for each class were mapped on the UAV image of Galibore. Throughout iterations, training samples were refined based on average size per class and visual inspection of preliminary results with the local ecology experts. This iterative process allowed for continuous improvement and refinement of the training samples.

Supervised classifiers need sufficiently large training samples to extract statistics from (Millard and Richardson, 2015). To ensure the classifier can extract statistics from the samples, a minimum of 25 pixels was established for each class, based on the PS imagery. With the 3m spatial resolution of PS imagery, the average area of the UAV-derived training samples for each class was aimed to be at least 225m^2. However, class proportionality was considered. For ecologically larger habitats (e.g, pools), the training samples were larger than in smaller habitats (e.g. rapids).

The average area was adjusted to reduce overfitting of the model to the training area. Based on visual assessment on the UAV image with the local ecology experts, training samples were adjusted to reduce overestimation of certain classes.

For visual assessment, a preliminary Random Forest model was trained on the Galibore area, using the PlanetScope bands cropped to the river boundary. Table 2.1 shows the hyperparameters used in training the Random Forest model [2].

Table 2.1. Random Forest model hyperparameters and data parameters

Hyperparameters			**Data parameters**	
Number of trees	Importance	Seed	Feature set	Target variable
100	permutation	0xfedbeef	Training samples	Habitat class

[2] The `ranger` package was used in R

2.5 Model training with different predictors

Three Random Forest models using different predictor combinations were trained on the Galibore area, then tested on Bheemeshwari and Mekedatu areas. The models were trained using the same hyperparameters from Table 2.1, and the final iteration training samples on the Galibore PS river boundary mask.

Literature has shown that adding textural features to the original bands as predictors can improve classification performance. However, radiometric and geometric quality can vary in PS imagery, due to small sensor size (Frazier and Hemingway, 2021). Therefore, the hypothesis is that using only textures could outperform the combination of bands and textures.

Texture layers represent different geostatistical measures of probability distribution of gray levels based on neighbouring pixels (Zheng et al., 2018, Pathak and Barooah, 2013). They are particularly valuable in riverine environments, where they could effectively differentiate between rapids and still water. The Haralick textures or grey-level co-occurrence matrices (GLCM) which were analyzed in this study are: contrast, dissimilarity, homogeneity, angular second moment (ASM), entropy, and variance. The mathematical formulas and interpretation for these textures can be seen in Table 2.2, based on Hall-Beyer (2017) and Hemalatha and Anouncia (2018).

Table 2.2. GLCM-based texture measures, their formulas, and their interpretation. N is the number of rows or columns in the gray-level co-ocurrence matrix; i is the row index; j is the column index; $P_{i,j}$ is the probability of neighboring cells to have gray levels $i\&j$.

Texture Measure	Formula	Measure of
Contrast	$\sum_{i,j=0}^{N-1} P_{i,j}(i-j)^2$	Local intensity variation
Dissimilarity	$\sum_{i,j=0}^{N-1} P_{i,j}\|i-j\|$	Difference between neighboring pixels
Homogeneity	$\sum_{i,j=0}^{N-1} \frac{P_{i,j}}{1+(i-j)^2}$	Closeness between neighboring pixels
Angular Second Moment (ASM)	$\sum_{i,j=0}^{N-1} P_{i,j}^2$	Uniformity or orderliness
Entropy	$\sum_{i,j=0}^{N-1} P_{i,j}[-\ln(P_{i,j})]$	Randomness or complexity
Variance (σ^2)	$\sum_{i,j=0}^{N-1} P_{i,j}(i-\mu)^2$	Spread of intensity values

Some textures highlight edges: contrast, dissimilarity, entropy, and variance. Other textures highlight patch composition: homogeneity and angular second moment.

To assess which texture metrics would be more suitable, a correlation analysis was performed on the Galibore extent of the image. Pearson correlation was computed for each pair of bands, and variance was computed for each band. Explained variance was computed to assess how much

each band contributes to the total variance. The formulas for correlation and variance analysis can be seen in Table 2.3.

Table 2.3. Metrics used for analysis. X and Y are the analyzed features; x_i and y_i are the individual pixels; $\bar{x}$ and $\bar{y}$ are the means of the features.

Metric	Formula
Correlation	$\text{Corr}(X,Y) = \frac{\sum(x_i-\bar{x})(y_i-\bar{y})}{\sqrt{\sum(x_i-\bar{x})^2\sum(y_i-\bar{y})^2}}$
Variance	$\text{Var}(X) = \frac{1}{n-1}\sum_{i=1}^{n}(x_i-\bar{x})^2$
Explained Variance	$\text{EV}(X) = \frac{\text{Var}(X)}{\sum \text{Var}(X_i)} \times 100$

To choose the most uncorrelated bands, the pairs with correlation higher than 0.85 or lower than -0.85 were compared in terms of variance. In each pair highly correlated pair, the band with the higher variance was kept, while the other was removed. Textural measures were computed on the most uncorrelated band with the highest variance. The same correlation and variance analysis was performed on these textures.

The following models were implemented:

1. All bands (blue, green, red and NIR) and uncorrelated textures
2. Only uncorrelated textures, computed on all bands (blue, green, red and NIR)
3. Uncorrelated bands and uncorrelated textures computed on uncorrelated bands

The first combination is suggested by literature, as textures have improved classification results in several habitat mapping tasks. The second combination is based on the hypothesis that using only textural features can be more robust, as bands can be affected by atmospheric hazing and spectral inconsistencies, especially in PS sensors. The third combination is based on the band correlation and variance analysis.

The variable importance for each model was assessed using the mean decrease in accuracy (Breiman, 2001). The permutation importance hyperparameter (Table 2.1) computes model accuracy when sequentially removing predictors from model training. The importance value is the percentage of accuracy decrease for each eliminated predictor compared to the model trained on all predictors (Breiman, 2001).

For each area, the predictor combinations were assessed with difference maps and class confusion statistics between models. The regions classified the same in all models were extracted for each study area. The region differently classified in at least 2 of the models is referred to as the model disagreement region. Within the disagreement region, similarities and differences between

each pair of models were analyzed. Habitat composition percentage of each model result was computed for the disagreement region to show classification differences per study area.

To assess class confusion, a change code was derived in the disagreement region for each pair of models, using **Equation 2.3**. The results of the models are values between 1 and 8, corresponding to the habitat classes (in alphabetical order). Therefore, the first digit of the change code represents the habitat classified by the first model, and the second digit to the results of the second model. Where digits are equal, it means that the models classified the pixel identically.

$$\text{Change code} = \text{Value}_{\text{model}_1} * 10 + \text{Values}_{\text{model}_2} \tag{2.3}$$

The change code raster value frequencies were computed for each model pair. On a coarse level, this showed how many pixels were classified the same between each pair of models (pixels with values 11, 22, ..., 88). On a more detailed level, the change codes showed how the pixels were classified differently between models. The values were converted to percentages, to showcase the class confusion between models for all pairs of habitat classes.

2.6 Accuracy assessment

Accuracy assessment is a challenging task in areas with low data availability conditions (Verbyla and Litvaitis, 1989). Studies such as Fallati et al. (2020) and Cho et al. (2014) assessed accuracy using direct observations on high-resolution remotely sensed data.

A stratified random point sampling strategy was employed for generating point validation datasets for Galibore, Bheemeshwari, and Mekedatu. Stratification was based on the classes, where additional validation points were added in underrepresented classes. Measuring random points directly in the field proved to be impractical, as some parts were highly inaccessible, which would have made the validation dataset unrepresentative for the entire region.

The validation datasets were created after the research team had seen preliminary results. Therefore, to avoid bias, the points were labelled by external annotators, instead of the research team. The annotators were asked to label all points and add points in underrepresented areas.

For **Galibore**, 200 random points were generated with a minimum distance of 50 meters between each pair of points, to ensure non-clustered distribution. The points were annotated using the UAV orthophoto. Prior to annotation, the points overlapping training areas were deleted, resulting in 183 points. The annotator added 18 additional points for *rapid*, and 12 additional points for *sand*, to obtain a more balanced validation dataset. The final validation dataset had 213 points (Figure 2.8).

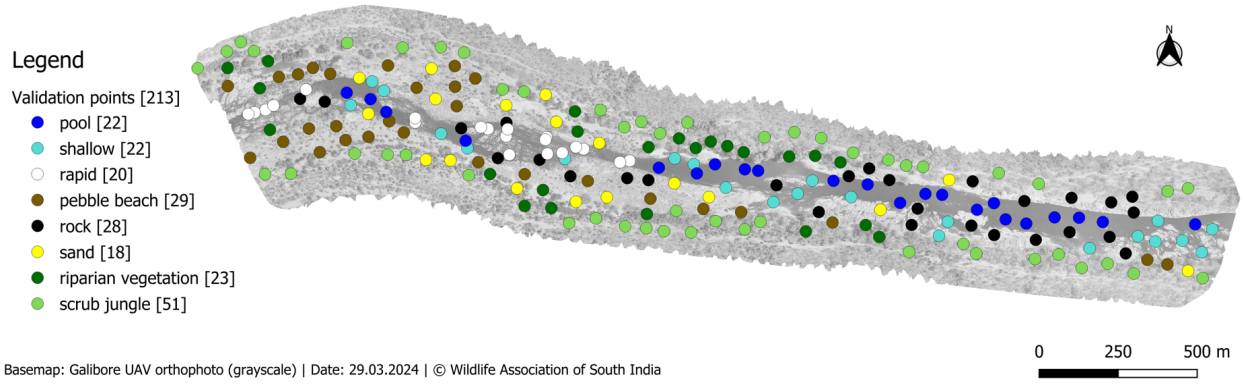

Figure 2.8. Labelled validation points on the UAV orthophoto of the Galibore area.

For **Bheemeshwari**, 250 random points were generated with a minimum distance of 50 meters between each pair of points. More points were generated in Bheemeshwari than in Galibore to account for difference in the surface of the study areas. The points were annotated on an Airbus image from 13.03.2024, available through Google Earth Pro. Airbus imagery has submeter resolution, making it suitable for extracting validation data (Pulighe et al., 2016). Moreover, the conditions are similar, since both the PlanetScope and Airbus image were collected in March. The annotator added 10 samples for *rapid*, 6 samples for *pebble beach*, and 6 samples for *sand*. The final validation dataset had 272 points (Figure D.1 in Appendix D).

In **Mekedatu**, a set of 250 random points was generated, with a minimum distance of 30m between each pair of points. The distance was adjusted in this case, because the river is narrower in Mekedatu, compared to Bheemeshwari and Galibore. The points were annotated on an Airbus image from 23.01.2022. The annotator added 18 samples for *sand* and 14 samples for *rapid*. The final validation dataset had 278 points (**Figure D.2** in **Appendix D**).

Accuracy assessment was performed on all models for Galibore, Bheemeshwari, and Mekedatu. The following metrics were considered: **recall**, **precision**, and **accuracy**. These metrics are calculated using the following values: true positives (TP), true negatives (TN), false positives (FP), and false negatives (FN). These values are computed and per class, using the confusion matrix between the results and the validation dataset of the area. To assess the overall model performance, the metrics were micro-averaged across all classes, per model and per area.

Given a validation set, for each class (X), the parameters are computed as in **Table 2.4**. True positives are pixels correctly classified as class X. False positives are pixels classified as class X, which in reality belong to other classes. False negatives are the the pixels which in reality belong to class X, but were wrongly assigned to other classes. True negatives are the pixels which neither belong to class X, nor were classified as such.

Table 2.4. Example of true and false positives and negatives on a class.

	Predicted: Class X	Predicted: Other class
Real: Class X	TP	FN
Real: Other class	FP	TN

Recall (**Equation 2.4**), captures the sensitivity of the model. It relates to the rate of predicted true positives within all positive samples in the validation dataset.

$$\text{Recall} = \frac{\text{TP}}{\text{TP} + \text{FN}} \tag{2.4}$$

Precision (**Equation 2.5**) shows how often the model is correct when predicting the target class. It relates to the rate of predicted true positives within all predicted instances of a class.

$$\text{Precision} = \frac{\text{TP}}{\text{TP} + \text{FP}} \tag{2.5}$$

Accuracy (**Equation 2.6**) shows the overall amount of correctly classified pixels. t considers all predicted true values of a class, relating to both the presence and the absence within the validation dataset.

$$\text{Accuracy} = \frac{\text{TP} + \text{TN}}{\text{TP} + \text{TN} + \text{FP} + \text{FN}} \tag{2.6}$$

Chapter 3

Results

3.1 Training samples

The training samples were created in three iterations. In each iteration, they were refined based on average sample area per class and preliminary visual assessment. For visual assessment, a preliminary Random Forest model was trained, using the bands of the PlanetScope image, cropped to the river boundary of the Galibore area.

The target average size per class was 225m^2. Figure 3.1 shows the average area (in m^2) per class for the training samples. For the *rapid* class, the average was still not met in the final iteration.

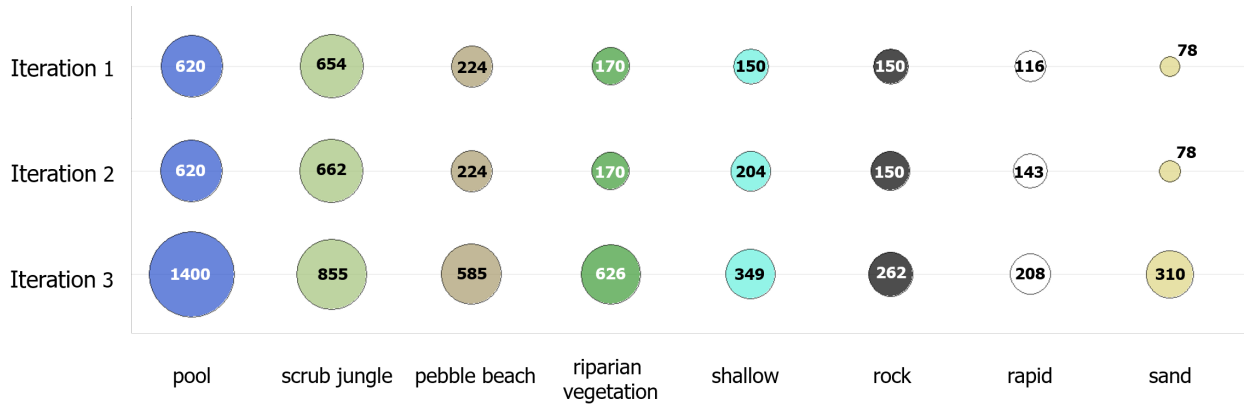

Figure 3.1. Comparison of average sample size per class across iterations. The bubble size and label represent average sample size per class (in m^2).

The training samples were also refined based on preliminary visual assessment with the local ecology experts. Figure 3.2 shows the results for the main areas which were considered in refining the training samples.

The first iteration consisted of the samples mapped with Naren Sreenivasan. In this iteration, results were particularly noisy. In *Area 2*, rocks and rapids were classified as pool, which was not valid according to local experts. In *Area 3*, shallow water was overestimated outside the main channel.

The second iteration corrected for *shallow* and *rapid* overestimation, based on visual assessment on the UAV image, together with Naren Sreenivasan. This is particularly visible in *Area 3*. However, results were still noisy, especially in *Area 2*. The size of the samples was not significantly modified in this step.

In iteration 3, habitats were clearly separated, with significantly reduced noise in the results, as visible in *Area 1*. Pools were classified more accurately according to local experts, as well as shallows and rapids (*Area 2*).

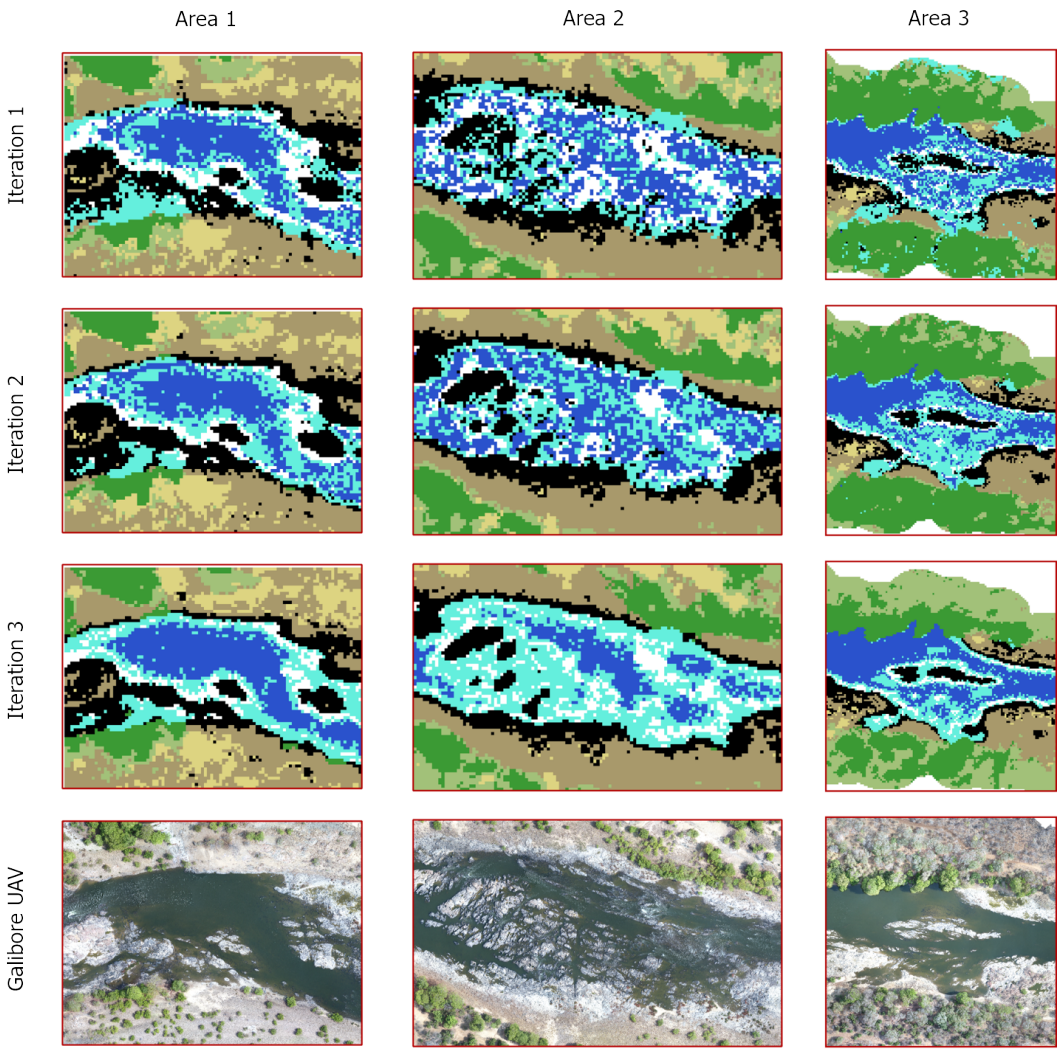

Figure 3.2. Visual comparison of preliminary results acorss training sample iterations.

The spatial distribution of the training samples in each iteration is shown in Figure 3.3. From iteration 1 to iteration 3, the number of samples decreased from 120 to 55, while the average area per class increased.

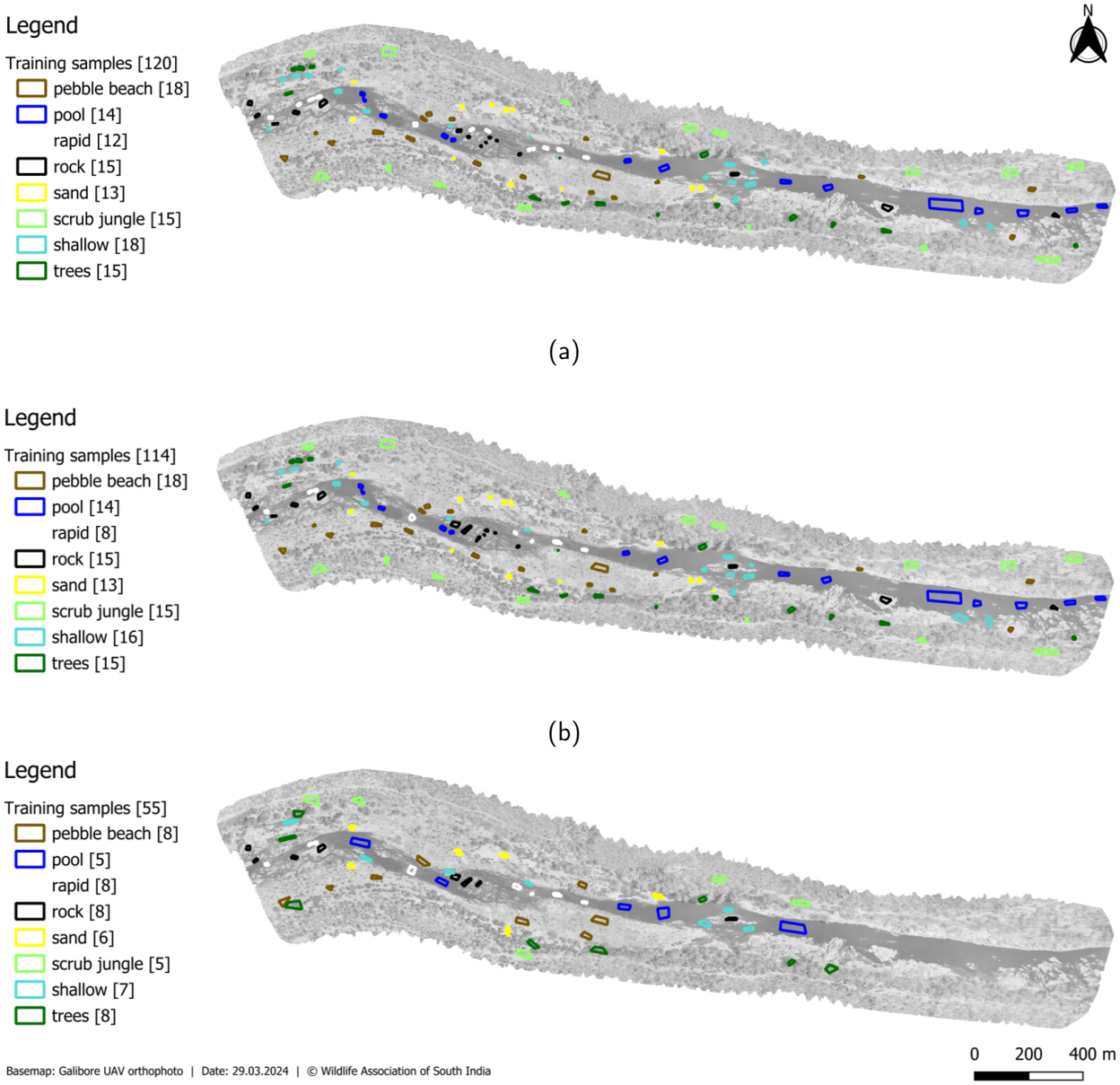

Figure 3.3. (a) Iteration 1; (b) Iteration 2; (c) Iteration 3.

3.2 Predictor choice

To assess which texture metrics would be more suitable, a correlation analysis was performed on the PlanetScope (PS) image section corresponding to the Galibore study area extent.

The Pearson correlation coefficients of the band pairs are shown in Figure 3.6a. Pairs with correlation higher than 0.85 or lower than -0.85 were compared in terms of band variance. In each highly correlated pair, the band with the highest variance was kept, while the other was discarded. Following the analysis, the **red** and **NIR** bands were uncorrelated, with NIR having the highest variance (Figure 3.6b).

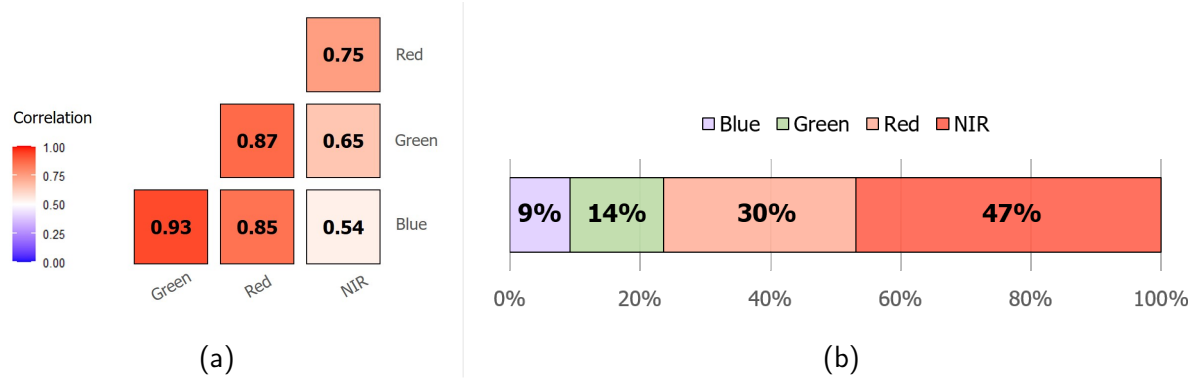

(a) (b)

Figure 3.4. Statistical relationships between PlanetScope bands in Galibore: (a) Pearson correlation; (b) Explained variance.

The same analysis was performed on textural measures computed on the NIR band (Figure 3.5). Textures were computed and analyzed only on the NIR band in this step, since it was the most uncorrelated band, with the highest variance. The following gray-level co-occurrence matrix (GLCM) textural features were considered: contrast, dissimilarity, homogeneity, angular second moment, entropy, and variance. Upon correlation (Figure 3.5a) and variance (Figure 3.5b) analysis, the following textural measures were found relevant: **homogeneity**, **entropy**, and **variance**.

Three models were created on the same training image and samples (third iteration), with different predictor combinations. A model was derived for each of the following predictor combinations:

1. **Model TB (textures and bands)**: all bands (blue, green, red, NIR), and the uncorrelated textures (homogeneity, entropy, variance) computed on all bands

2. **Model T (only textures)**: uncorrelated textures (homogeneity, entropy, variance) computed on all bands

3. **Model NIR-R (only red and NIR bands and textures)**: red and NIR bands, and uncorrelated textures (homogeneity, entropy, variance) computed on red and NIR bands

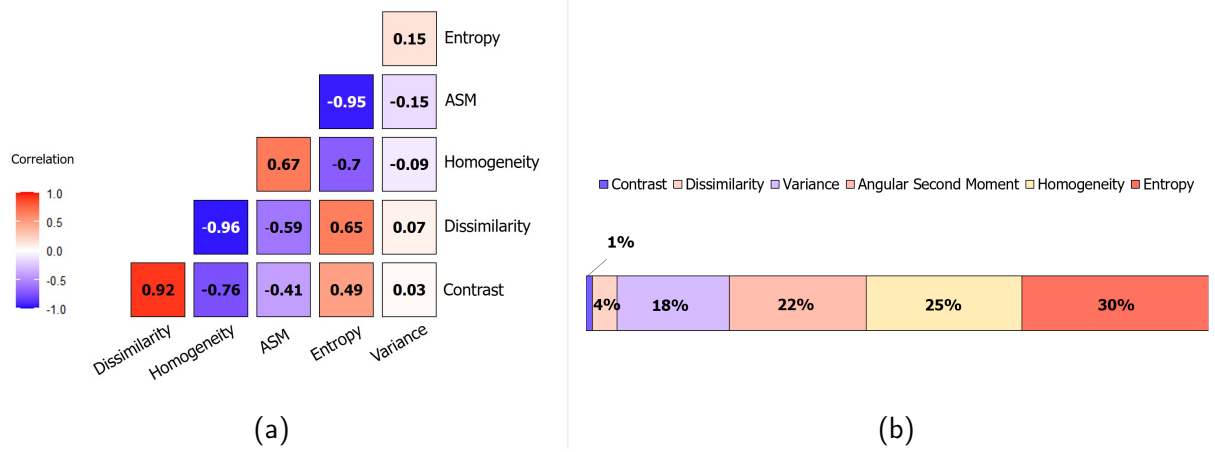

(a) (b)

Figure 3.5. Statistical relationships of textures on the PlanetScope NIR band in Galibore: (a) Pearson correlation; (b) Explained variance.

For each model, the variable importance can be seen in **Figure 3.6**. For all models, variance of the red band (Var R) was the most important predictor, with the highest overall importance in model T. Homogeneity and entropy for all bands had low importance in all models. In models TB and T, variance of the green band had relatively high values as well.

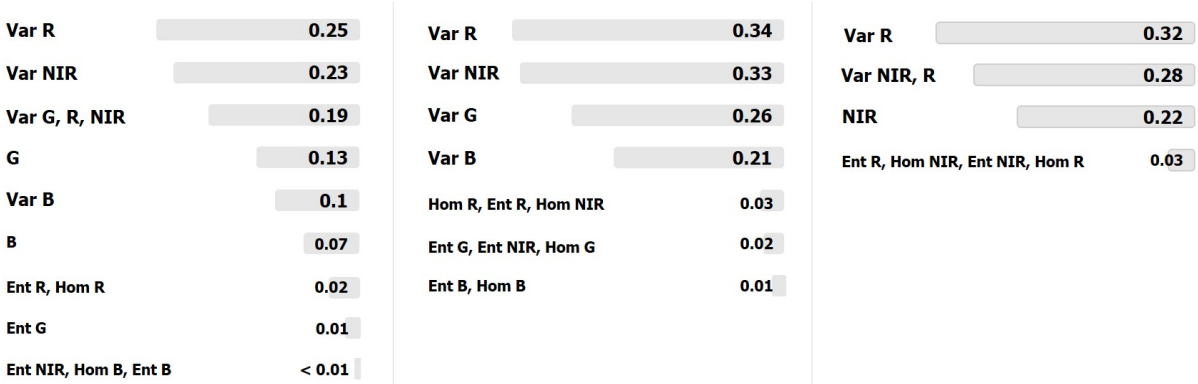

(a) (b) (c)

Figure 3.6. Variable importance of (a) Model TB; (b) Model T; (c) Model NIR-R. Notations: Var (variance), Hom (homogeneity), Ent (entropy), R (red band), NIR (near-infrared band), G (green band), B (blue band).

The following sections show the comparison between the results of models T, TB and NIR-R, in Galibore, Bheemeshwari, and Mekedatu. The results focus on how habitats are classified similarly and differently between models for each area.

3.2.1 Galibore

Figure 3.7a shows the similarities and differences in model classification results. The areas equally classified, shown as the habitats, consist of 79% of the image. The red areas show model disagreement regions, containing pixels classified differently by at least two models (21%).

Figure 3.7b shows pairwise similarities between models within the red area. Results of models TB and T show the highest overlap. The lowest similarity is between models TB and NIR-R.

The individual maps corresponding to each model are shown in Figure E.1 of Appendix E.

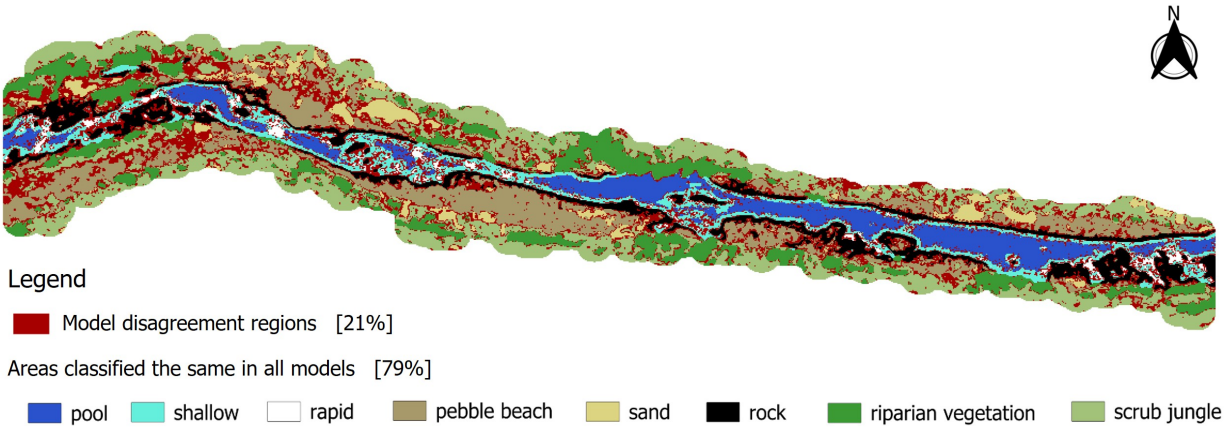

(a)

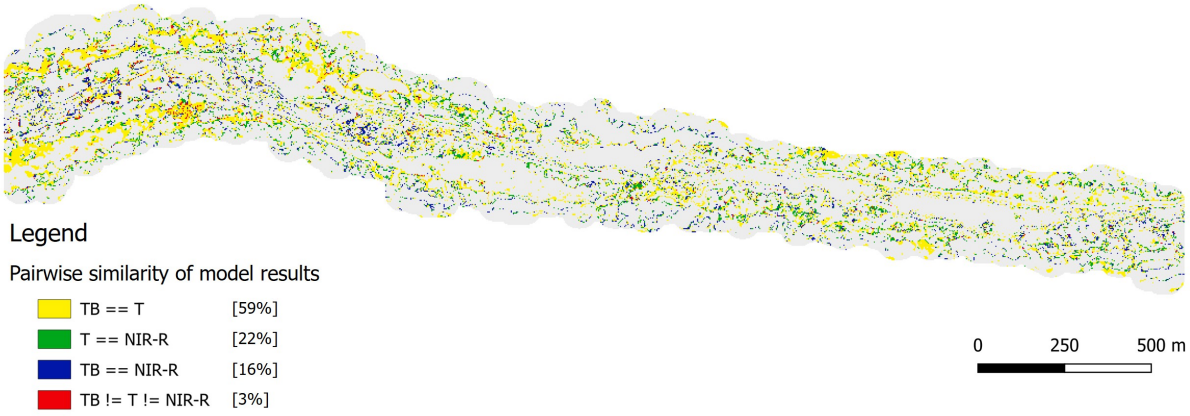

(b)

Figure 3.7. (a) Classification results and differences between models in Galibore. Areas classified the same by all models are shown as habitat classes. Model disagreement areas are shown in red. (b) Pairwise similarity between models and their percentage of the red area in Galibore. The map shows model agreement between pairs of models (yellow, green, blue), and pixels classified differently by all models (red).

Figure 3.7b also reveals the nature of the difference between models. The yellow area, where NIR-R results differ from TB and T results, has the highest surface area and compactness. The green area and the blue area (where results of TB, respectively T are different from all other models) have a more dispersed pixel distribution. This shows that differences between NIR-R results and T and TB results tend to have a pattern, while for the other models differences tend to be more random.

Figure 3.7a shows the habitat percentage for each model within the model disagreement region. Figure 3.7b reveals how habitats are classified differently between models.

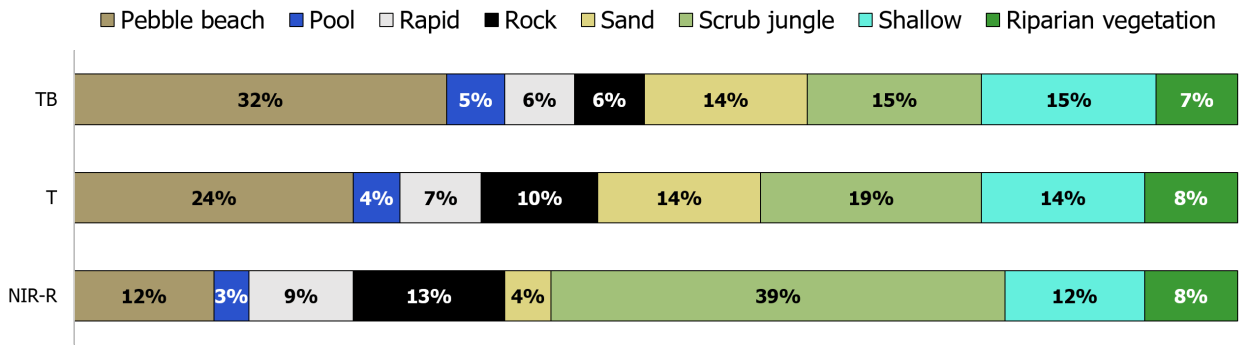

(a)

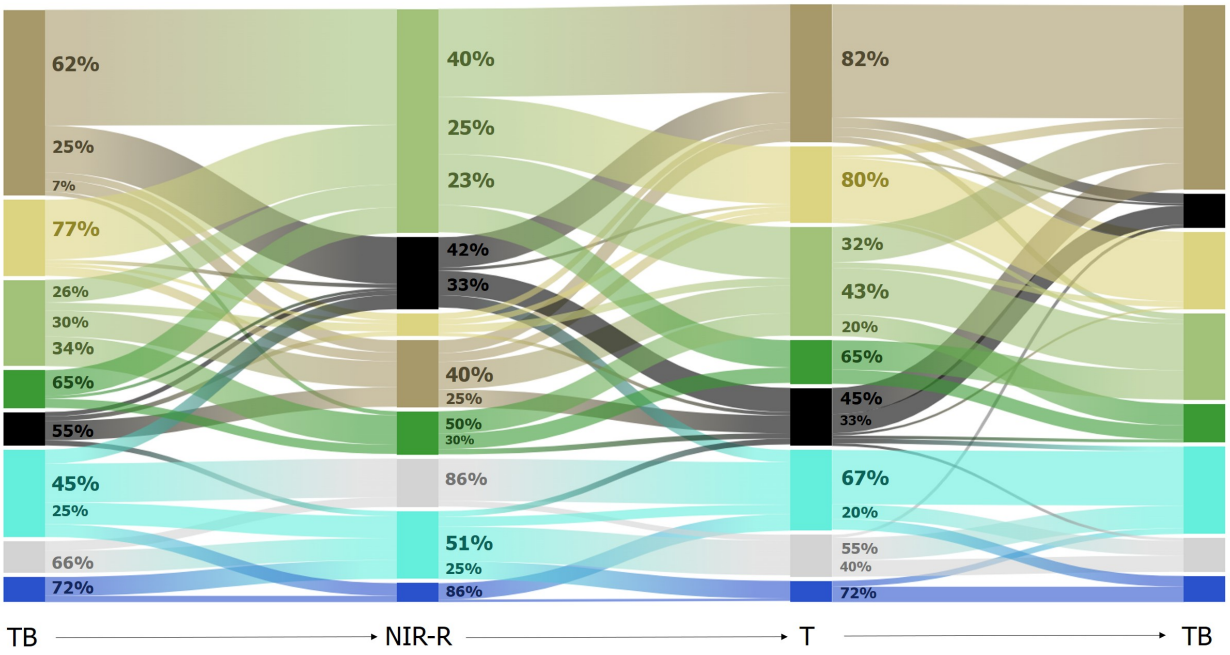

(b)

Figure 3.8. (a) Habitat composition for each model in the disagreement region in Galibore (red area in Figure 3.7a). (b) Class confusion between models in the disagreement region in Galibore.

The highest differences can be seen in: pebble beach, rock, sand, and scrub jungle. The overall differences between models TB and T are lower than between TB and NIR-R, and T and NIR-R.

Figure 3.8a shows that model TB classifies the largest amount of pebble beach among all models, while model NIR-R classifies the largest amount of scrub jungle among all models. **Figure 3.8b** shows that there is high class confusion between pebble beach and scrub jungle between NIR-R and the other models (62% with TB, and 40% with T). Between results of models TB and T, the majority of pebble pixels are classified the same. A similar pattern can be observed between sand and scrub jungle. The NIR-R model tends to classify pixels as scrub jungle that models T and TB classify as sand.

The results of model NIR-R have the highest amount of rock relative to the other models (**Figure 3.8a**). The most common class confusion occurring is with pebble beach. Moreover, there is class confusion between rock and shallow between results of models NIR-R and T (25%). This pattern is only marginally present between results of the other models.

There is high class confusion between shallow and rapid pixels in all models. More than half of pixels classified as shallow by model TB are classified as rapid by model NIR-R. Conversely, a majority of pixels classified as rapid by NIR-R are classified as shallow by T. There is more overlap between the results of models T and TB for shallows, but the class confusion is still high.

Pools show high class confusion in the results of model NIR-R, compared to results of TB and T. The majority of pixels classified as pool by model TB are classified as shallow by model NIR-R. The same pattern is visible between results of models NIR-R and T. There is a high overlap between the results of models T and TB, which classify the majority of pool pixels the same.

3.2.2 Bheemeshwari

Figure Figure 3.9a shows areas equally classified in all models (76%) and the model disagreement regions, which are areas classified differently by at least two models (24%). Figure Figure 3.9b shows pairwise result overlap between models in the disagreement region. Similarly to Galibore, results of models TB and T have the highest overlap.

The individual maps corresponding to each model are shown in Figure E.2 of Appendix E.

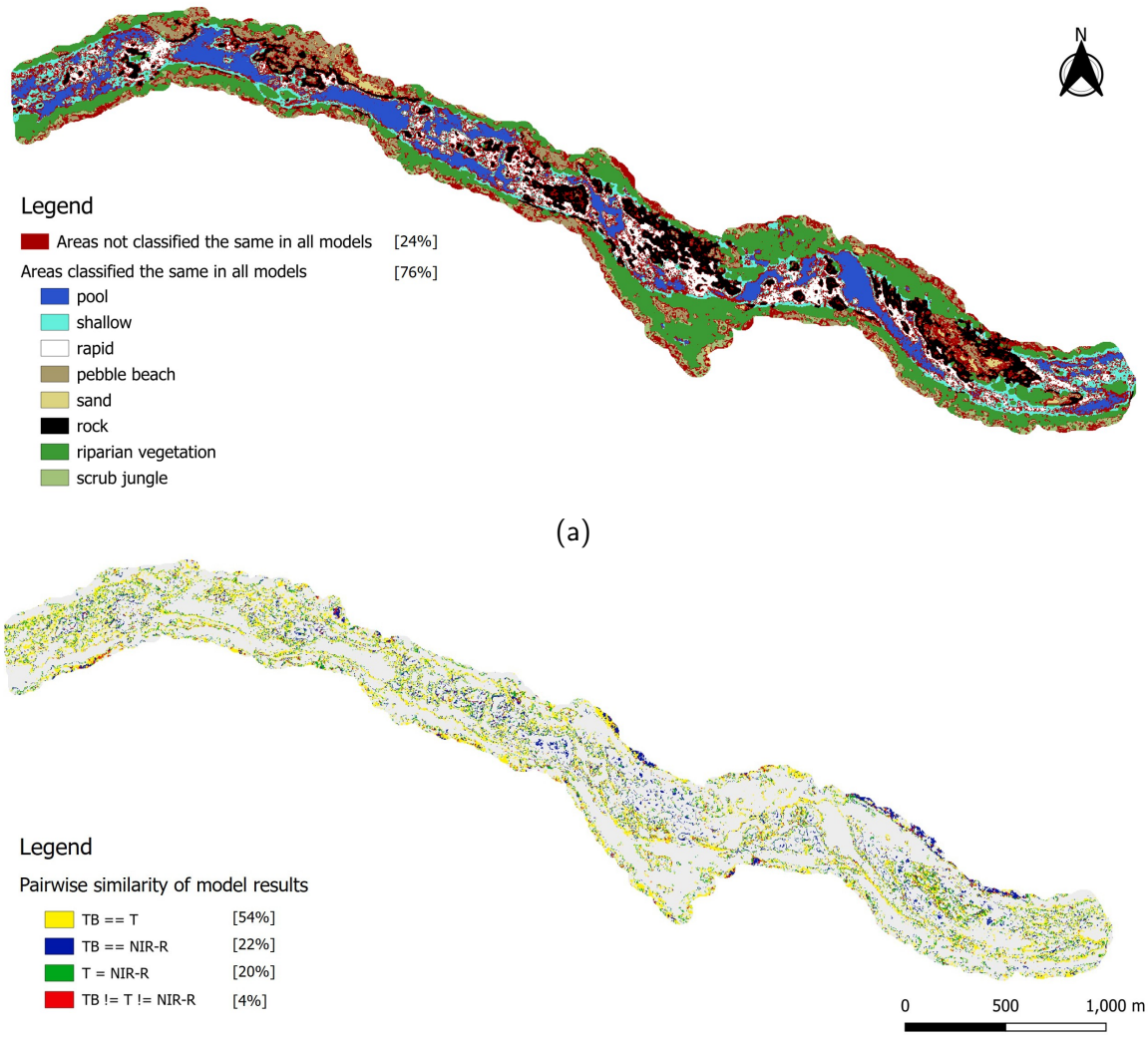

Figure 3.9. (a) Classification results and differences between models in Bheemeshwari. Areas classified the same by all models are shown as habitat classes. Model disagreement areas are shown in red. (b) Pairwise similarity between models and their percentage of the red area in Bheemeshwari. The map shows model agreement between pairs of models (yellow, green, blue), and pixels classified differently by all models (red).

Based on the spatial distribution of pixels in Figure 3.9b, the difference type can be identified. The yellow areas show where model NIR-R had different results than both other models. The blue areas show where model T has different results. The green area shows where model TB has different results. Red areas show where pixels were classified differently in all models. Compact spatial patterns can be seen in the yellow and blue areas, while the green pixels have a more random distribution.

Figure 3.10a shows the habitat percentage for each model within the red area. Figure 3.10b shows how habitats are differently classified between models.

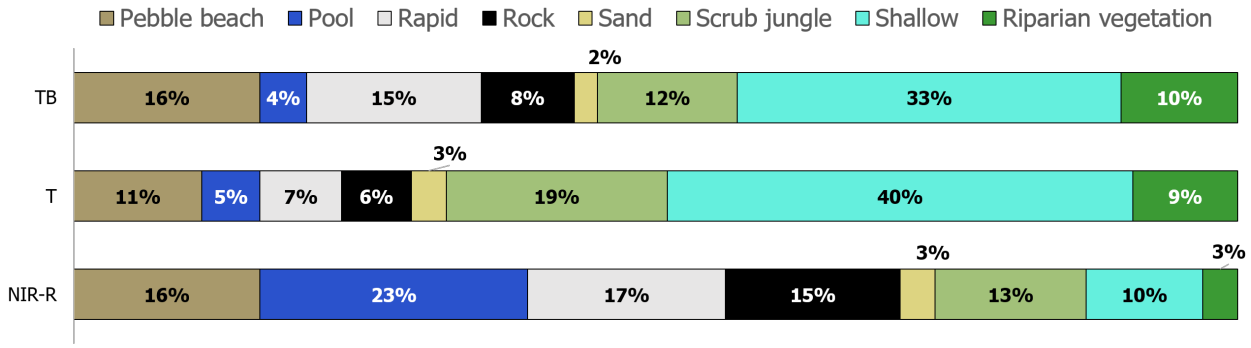

(a)

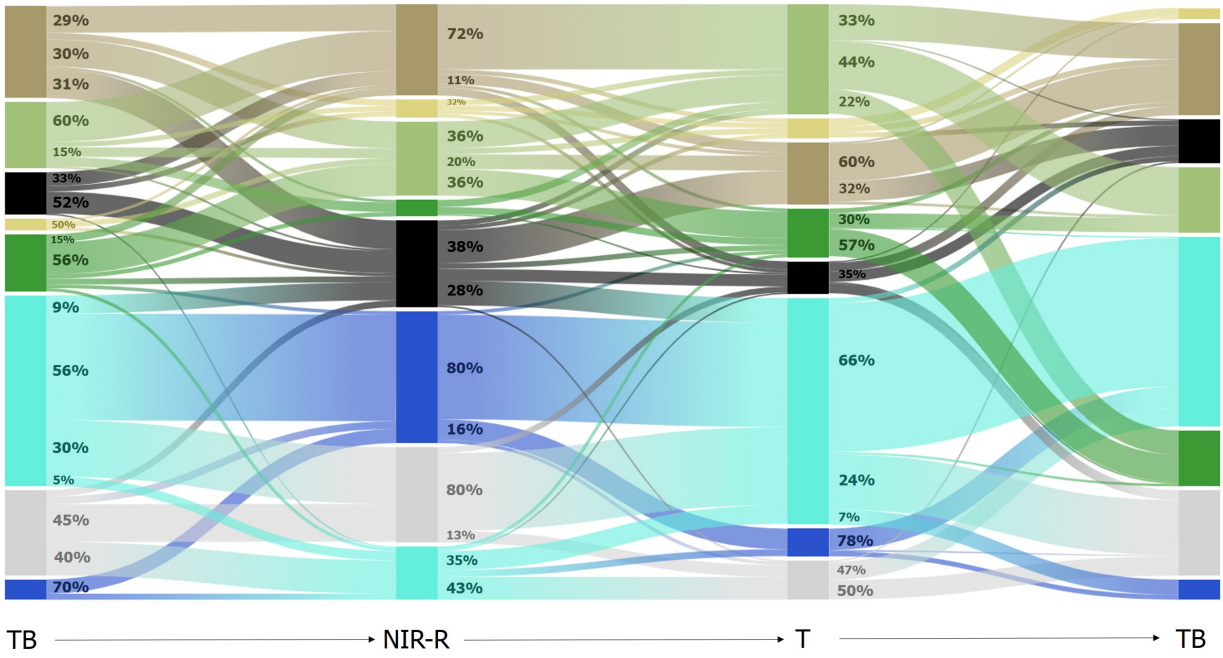

(b)

Figure 3.10. (a) Habitat composition for each model in the disagreement region in Bheemeshwari (red area in Figure 3.9a). (b) Class confusion between models in the model disagreement region in Bheemeshwari.

Contrary to Galibore, the results in Bheemeshwari are more similar in terms of scrub jungle, pebble beach, and sand. However, higher differences can be observed in the shallow, pool, rapid, and rock habitats.

Shallow represents 40% of the disagreement region in results of model T, and only 10% in results of model NIR-R (**Figure 3.10a**). **Figure 3.10b** shows that a majority of pixels classified as shallow by model T are classified as pool by model NIR-R. This also correlates with the high percentage of pool in the results of model NIR-R. The majority of pixels classified as pool by model NIR-R were classified as shallow by model T. Meanwhile, results of models T and TB show a high overlap for shallow.

Figure 3.10a shows that results of model T have a significantly lower amount of rapid pixels compared to the other models. **Figure 3.10b** reveals that a majority of pixels classified as rapid by model NIR-R are classified as shallow by model T. The highest similarity is between results of models T and TB, while the lowest is between results of models NIR-R and T.

Rock has similar class confusion patterns with Galibore. A large amount of pixels classified as rock by model NIR-R are classified as shallow by model T. However, contrary to Galibore, there is higher class confusion between rock and rapid, especially between results of models T and TB.

Contrary to Galibore, scrub jungle has the highest percentage in results of model T. A majority of pixels classified as pebble beach by model NIR-R are classified as scrub jungle by model T. Consversely, a third of pixels classified as scrub jungle by model T are classified as pebble beach by model TB.

3.2.3 Mekedatu

Figure 3.11a shows areas where pixels were classified the same by all models (66% of all pixels) and the model disagreement region (34%).

Figure 3.11b shows the pairwise similarity between model results within the model disagreement regions. Results of models T and TB show the highest overlap. The lowest similarity is between models T and NIR-R.

The individual maps for each model are shown in Figure E.3 of Appendix E.

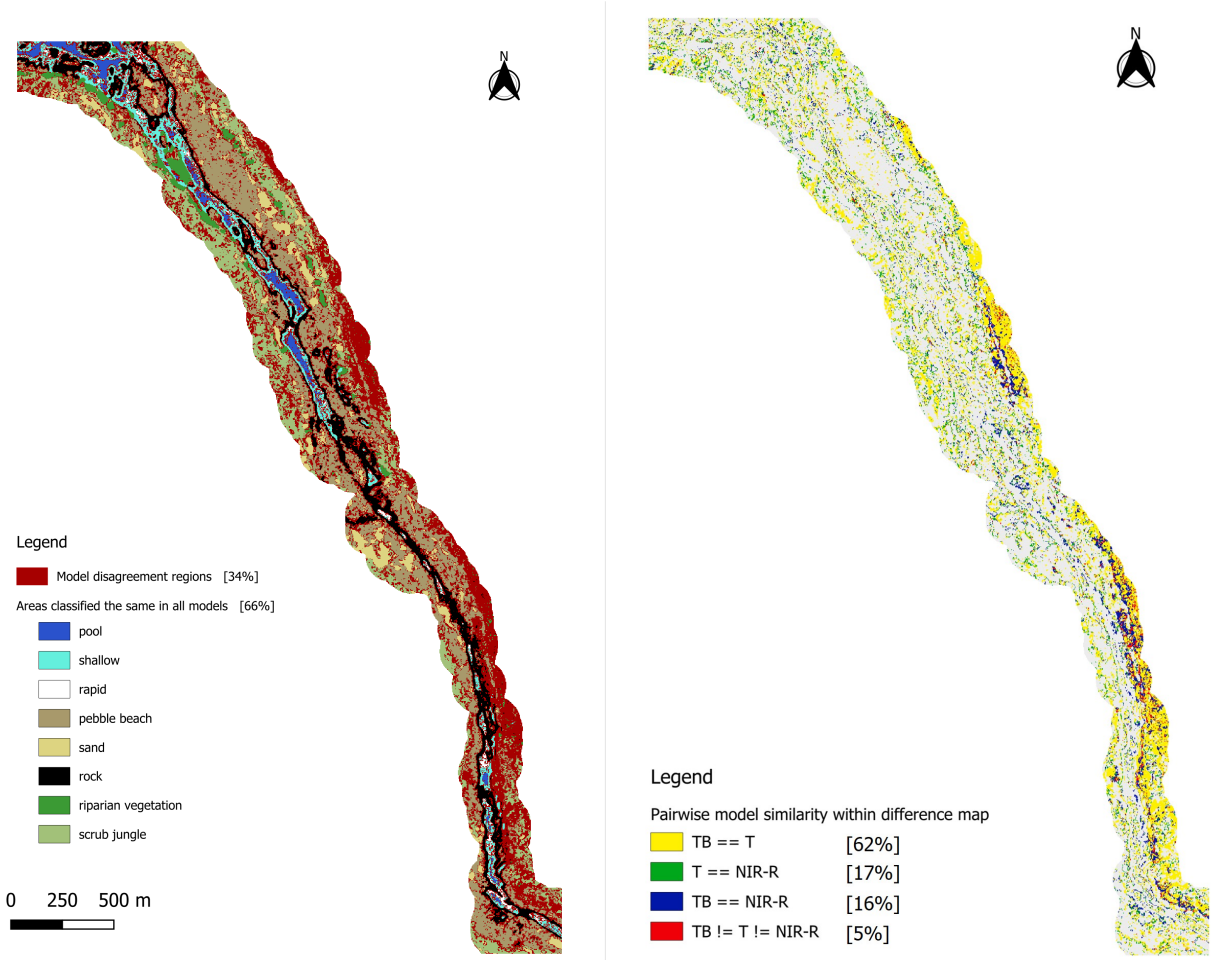

(a) (b)

Figure 3.11. (a) Classification results and differences between models in Mekedatu. Areas classified the same by all models are shown as habitat classes. Model disagreement areas are shown in red. (b) Pairwise similarity between models and their percentage of the red area in Mekedatu. The map shows model agreement between pairs of models (yellow, green, blue), and pixels classified differently by all models (red).

The change patterns show that the results of model NIR-R are the most different from both models T and TB (yellow areas). The spatial pattern is clustered, showing systematic differences. The more dispersed spatial distribution of green and blue areas show that the difference between results of models T and TB are more random.

Figure 3.12a shows the habitat percentage for each model within the red area. Figure 3.12b shows how habitats are differently classified between models.

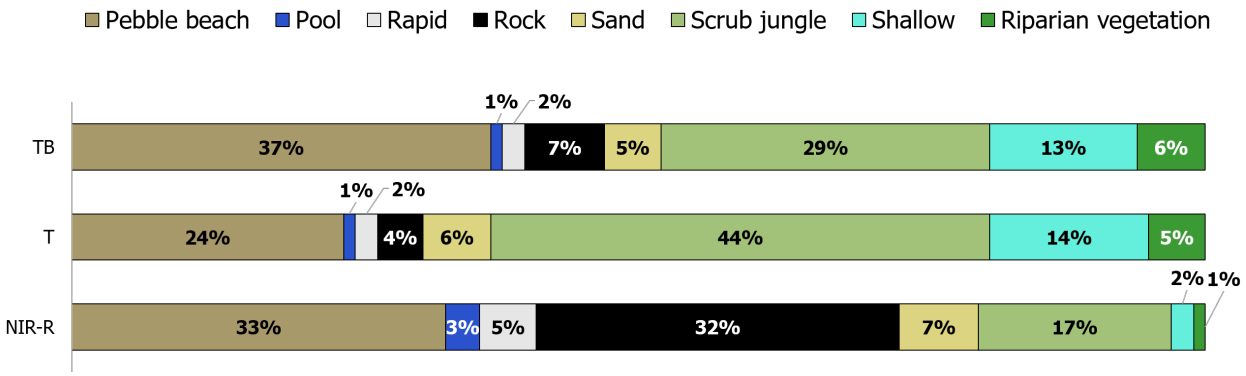

(a)

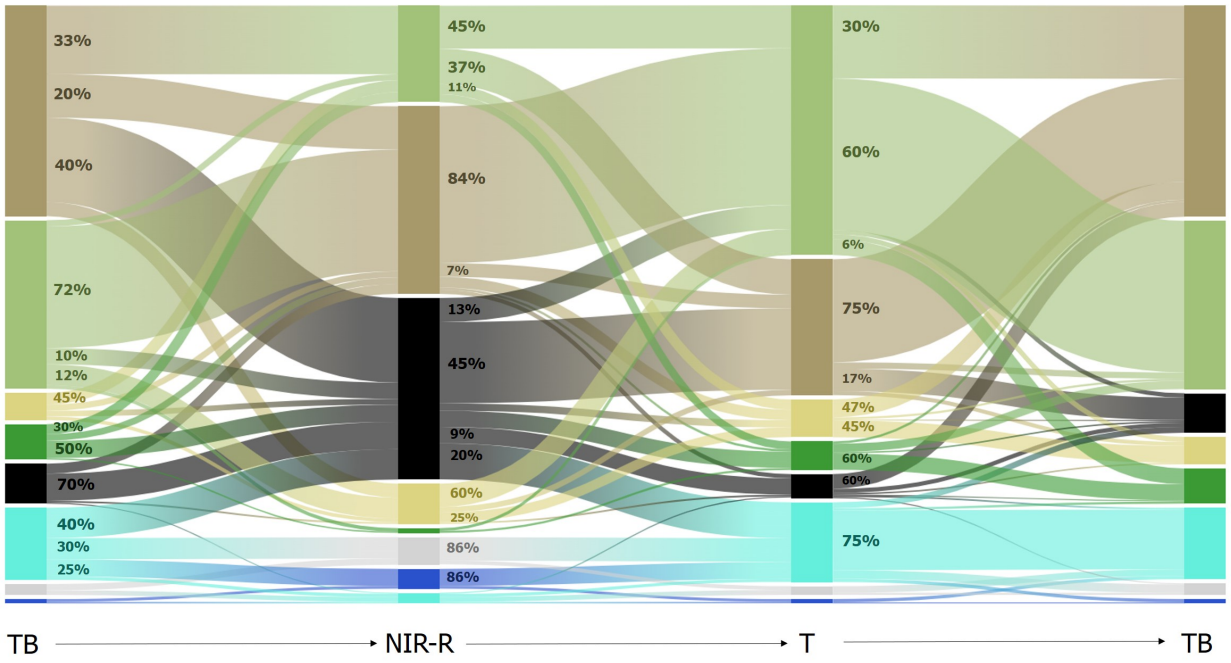

(b)

Figure 3.12. (a) Habitat composition for each model in the disagreement region in Mekedatu (red area in Figure 3.11a). (b) Class confusion between models in the disagreement region in Mekedatu.

Scrub jungle is the habitat showing the most difference in Mekedatu (**Figure 3.12a**). However, contrary to Galibore and similarly to Bheemeshwari, scrub jungle has the highest percentage in results of model T. The majority of pixels are classified the same as scrub jungle between models T and TB. However, most of the pixels classified as pebble beach by model NIR-R are classified as scrub jungle by model T.

Similarly to Galibore, pebble beach has the highest percentage in results of model TB. A low percentage of pebble beach pixels are classified the same by models NIR-R and T. Between results of models T and TB, the majority of pebble beach pixels are classified the same. However, in Mekedatu, pebble beach is mainly confused with rock instead of scrub jungle.

Model NIR-R classifies the highest amount of rock relative to the other models (**Figure 3.12a**). Between models NIR-R and T, almost half of the rock pixels are confused with pebble beach.

A similar pattern to Bheemeshwari is present in Mekedatu regarding shallow-rock class confusion between results of model NIR-R and the others. Almost half of pixels classified as shallow by model TB are classified as rock by model NIR-R. Conversely, 20% of pixels classified as rock by NIR-R are classified as shallow by T. Between results of models T and TB, there is little class confusion between shallow and rock, and a majority of shallow pixels overlap.

3.3 Accuracy assessment

Accuracy assessment is performed using labelled points for Galibore, Bheemeshwari, and Mekedatu. Table 3.1 shows the micro-averaged metrics of all classes and areas per model. All scores were computed using the confusion matrices of each model and area, which are available in Appendix F. Model T had the highest scores on average, closely followed by model TB. Model NIR-R had the lowest scores on average. However, on average, models T and TB are similar.

Table 3.1. Micro-averaged scores of all classes and areas per model.

Model	Recall & Precision	Overall
TB	0.55	0.89
T	0.56	0.89
NIR-R	0.49	0.87

Table 3.2 shows the micro-averaged scores of all classes by area and model. By area, model T outperformed the other models in Galibore and Bheemeshwari. In Mekedatu, precision and recall are larger in model TB, but only by 0.1 compared to model T.

Table 3.2. Micro-averaged scores of all classes per area and model

Area	Model	Recall & Precision	Accuracy
Galibore	TB	0.6	0.9
	T	0.62	0.91
	NIR-R	0.56	0.89
Bheemeshwari	TB	0.57	0.89
	T	0.58	0.9
	NIR-R	0.52	0.88
Mekedatu	TB	0.49	0.87
	T	0.48	0.87
	NIR-R	0.4	0.85

For a more detailed assessment, accuracy metrics computed by class for each model and area are shown in the following sections.

3.3.1 Galibore

The accuracy metrics by model and habitat for Galibore can be seen in Figure 3.13.

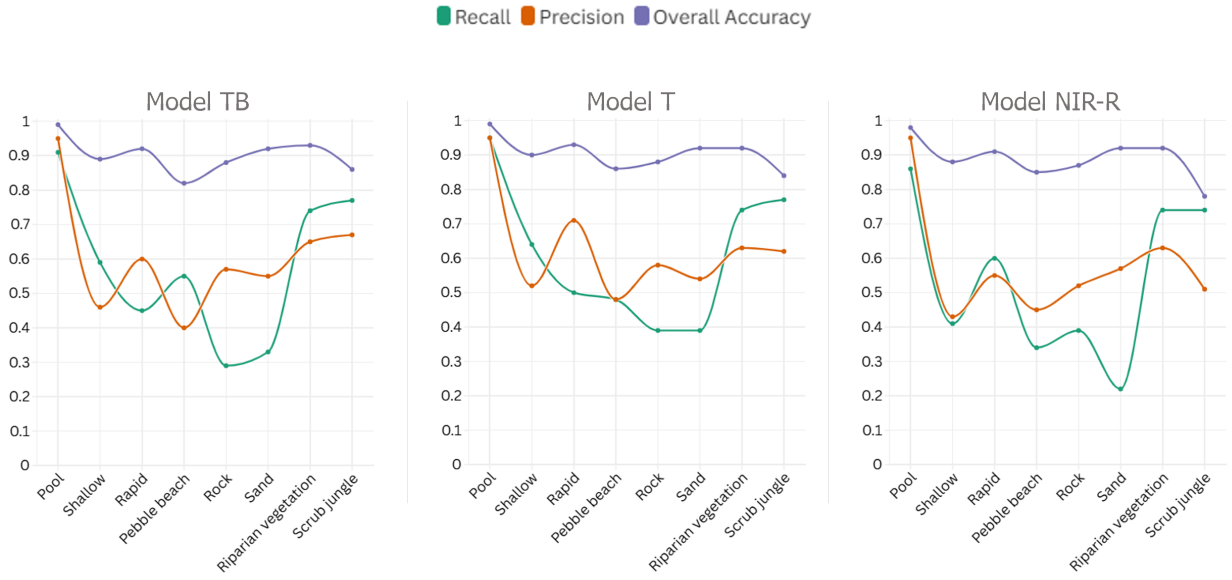

Figure 3.13. Accuracy metrics by model and habitat for Galibore.

Pool has the highest accuracy scores by habitat in all models. Model T has the highest scores: 0.99 accuracy, and 0.95 recall and precision. **Shallows** have the highest scores in model T: 0.9 accuracy, 0.65 recall, and 0.51 precision. **Rapids** have the highest scores in model T: 0.93 accuracy, 0.7 precision and 0.5 recall.

Pebble beach has the highest accuracy in model T (0.86), followed by model NIR-R (0.85) and model TB (0.82). Model T shows the most balanced results: 0.49 for both recall and precision. Even though recall is higher in model TB (0.55), both accuracy (0.82) and precision (0.4) are lower. **Rock** has the highest scores in model T: 0.88 accuracy, 0.59 precision, and 0.4 recall. **Sand** has 0.91 accuracy in all models. Precision is the highest in model NIR-R (0.57), but the recall is significantly lower (0.21). Model T shows the most balanced results: 0.54 precision and 0.4 recall.

Riparian vegetation has similar values in all models. Accuracy is 0.92, and recall is 0.74 in all models. Model TB shows the highest precision (0.65). **Scrub jungle** has the highest scores in model TB: 0.86 accuracy, 0.78 recall, and 0.68 precision.

Overall and per class, model T had the highest overall accuracy scores in Galibore. The habitat map generated by model T in Galibore is shown in Figure Figure 3.14.

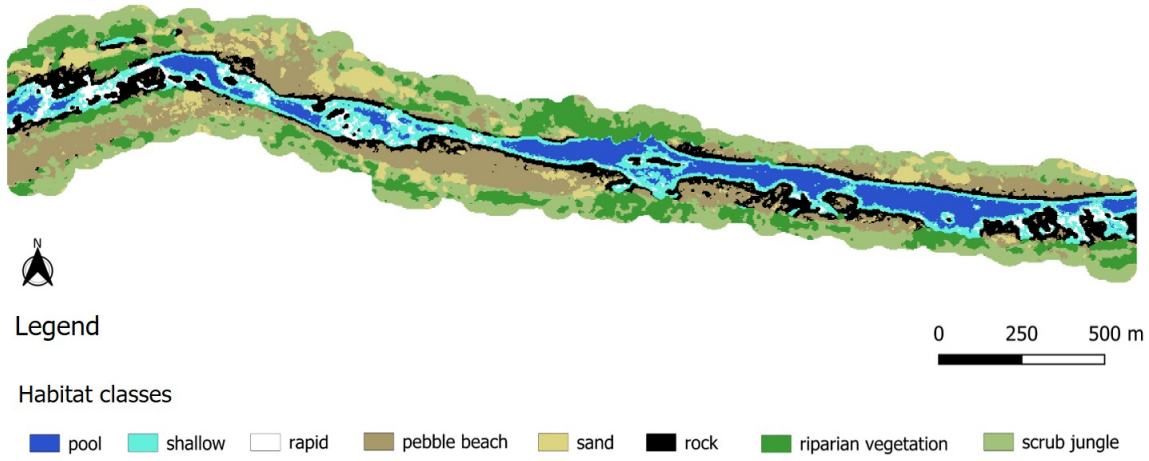

Figure 3.14. Habitat map generated by model T in Galibore.

Several misclassified areas were found, compared to the validation points. For example, Figure 3.15 shows misclassified rock points in the classification results of model T. The results of the other models are not shown, because they show similar patterns. Some rock points are classified as rapids, while some are classified as pebble beach.

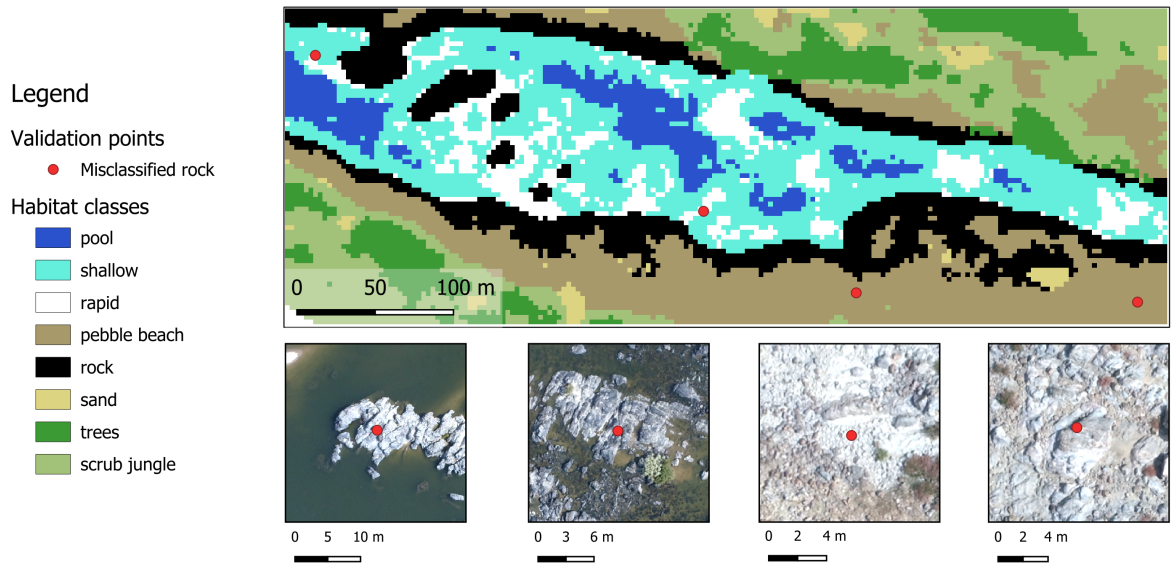

Figure 3.15. Misclassified rock points in Galibore. The figure shows classification results for model T, and zoomed-in sections of the UAV image. The UAV sections are in the same order as the points on the classification map, from left to right.

3.3.2 Bheemeshwari

The accuracy metrics for Bheemeshwari using point validation data can be seen in **Figure 3.16**.

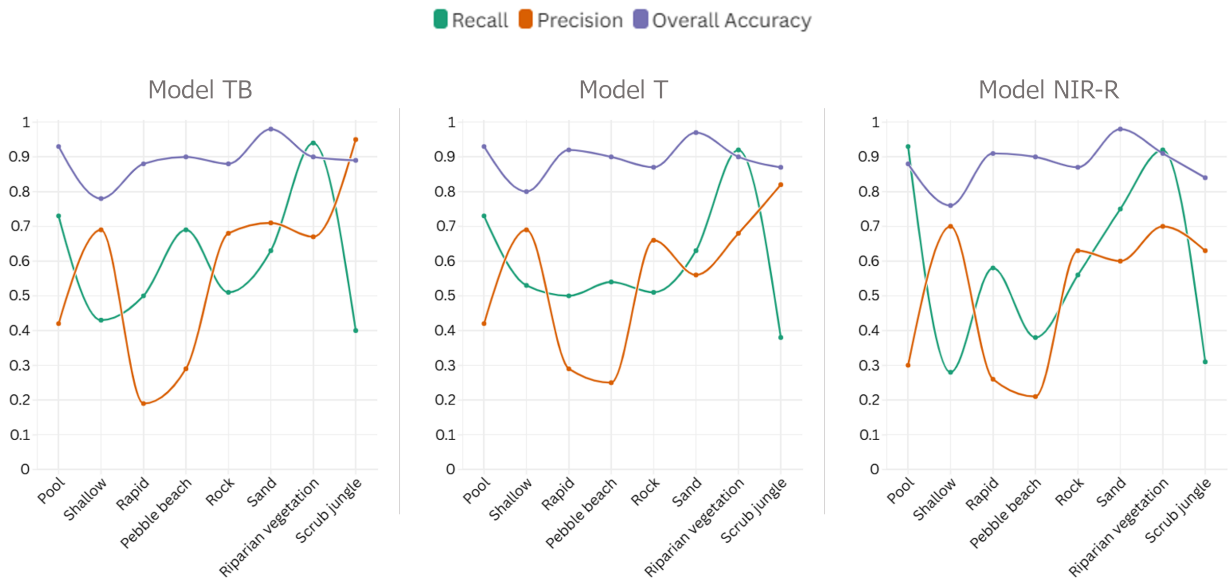

Figure 3.16. Accuracy metrics by model and habitat for Bheemeshwari.

Pool has high accuracy in the results of all models ($\geq$ 0.85). In models TB and T, values are equal for recall (0.73) and precision (0.42). In model NIR-R, recall is 0.94, and precision is 0.3. **Shallow** has the highest accuracy metrics in model T: 0.8 accuracy, 0.7 precision, and 0.52 recall. Precision is the same in all models, but recall and accuracy are the highest in model T and lowest in model NIR-R. **Rapid** has the highest metrics in model T: 0.9 accuracy, 0.5 recall, and 0.3 precision. Accuracy and recall are the same in all models, but precision is higher than in models NIR-R (0.25) and TB (0.2).

Pebble beach has the highest scores in model TB: 0.9 accuracy, 0.7 recall, and 0.3 precision. Recall is significantly lower in models T (0.55) and NIR-R (0.4). **Rock** has the highest metrics in model TB: 0.87 accuracy, 0.7 precision, and 0.5 recall. However, the results are not significantly lower in the other models. **Sand** has the same overall accuracy in all models (0.98), but different recall and precision values. Model TB has the highest precision (0.7), while model NIR-R has the highest recall (0.75). On average, model NIR-R has the highest scores.

Riparian vegetation has the highest scores in model TB: 0.9 accuracy, 0.94 recall, and 0.67 precision. However, results are similar in all models. **Scrub jungle** has the highest metric values in model TB: 0.95 precision, 0.9 accuracy and 0.4 recall. Both T and NIR-R models show a significant decrease in precision.

In Bheemeshwari, model T had the highest overall accuracy scores. The habitat map generated by model T in Bheemeshwari is shown in Figure **Figure 3.17**.

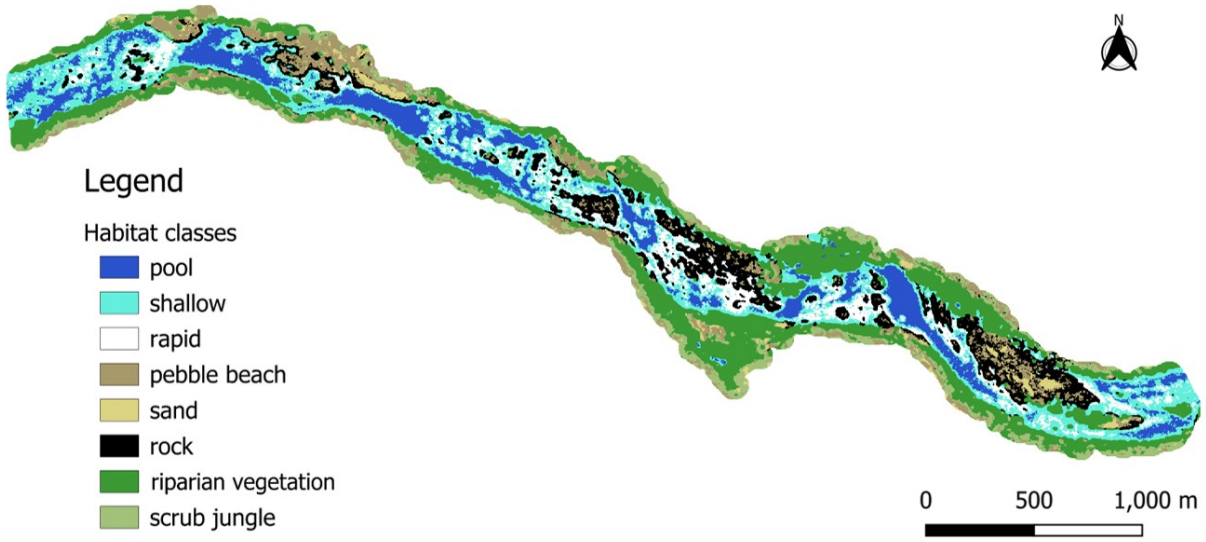

Figure 3.17. Habitat map generated by model T in Bheemeshwari.

3.3.3 Mekedatu

The accuracy metrics for Mekedatu using point validation data can be seen in Figure 3.18.

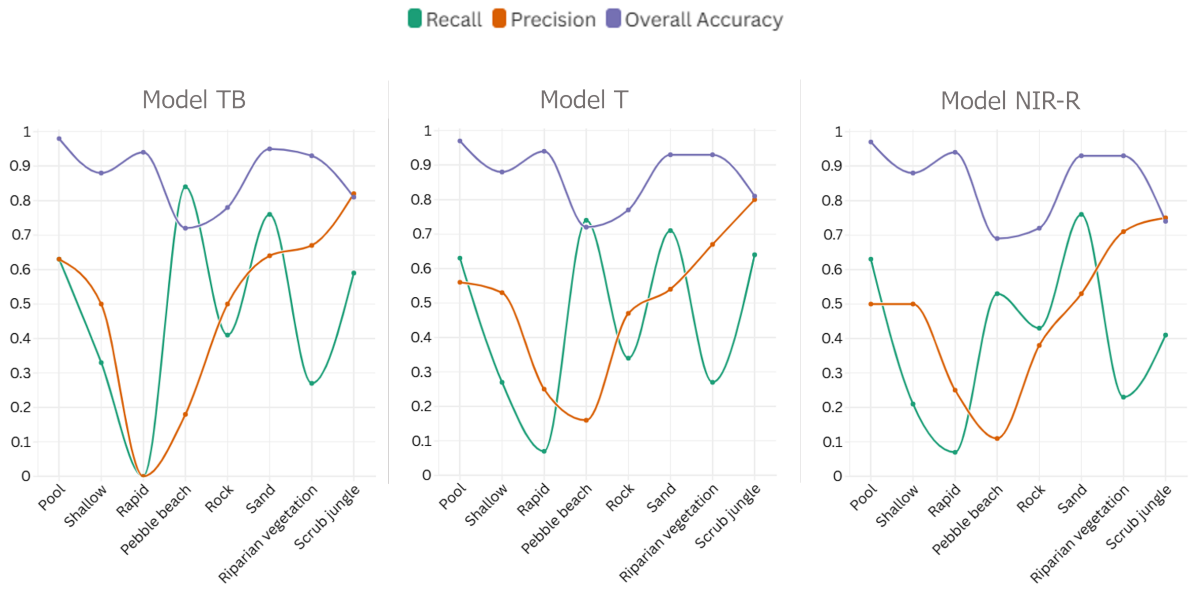

Figure 3.18. Accuracy metrics by model and habitat for Mekedatu.

Pool has the highest metrics in model TB: 0.99 accuracy, and 0.63 precision and recall. Precision decreases visibly in models T and NIR-R, while recall is constant. **Shallow** has 0.8 accuracy in all models, and lower recall than precision. Model T has the highest precison (0.52), while model TB has the highest recall (0.32). On average, model TB has the highest accuracy metrics, as the recall value is higher relative to the other models than precision. **Rapid** has 0.94 accuracy in all models. Models T and NIR-R have the same precision (0.25) and recall (0.18) values. On the other hand, model TB showed 0 for both precision and recall.

Pebble beach has the highest metrics in model TB: 0.72 accuracy, 0.85 recall, and 0.29 precision. Accuracy is the lowest among all habitats in all models. **Rock** has the highest metrics in model TB: 0.79 accuracy, 0.5 precision, and 0.4 recall. Recall is slightly higher in model NIR-R (0.42), but precision is significantly lower (0.38). **Sand** has the highest scores in model TB: 0.93 accuracy, 0.77 recall, and 0.63 precision.

Riparian vegetation has similar results in all models. Overall accuracy is 0.92 in all models. Precision is the highest in model NIR-R (0.7), while recall is highest in models TB and T (0.28). On average, model NIR-R has higher scores. **Scrub jungle** has the highest scores in model T: 0.8 accuracy and precision, and 0.65 recall. Models TB and T have significantly lower recall values.

In Mekedatu, models TB and T had similar overall accuracy scores. Per class, model T showed more balanced performance in classifying individual habitats, such as rapids. The habitat map generated by model T in Mekedatu is shown in Figure **Figure 3.19**.

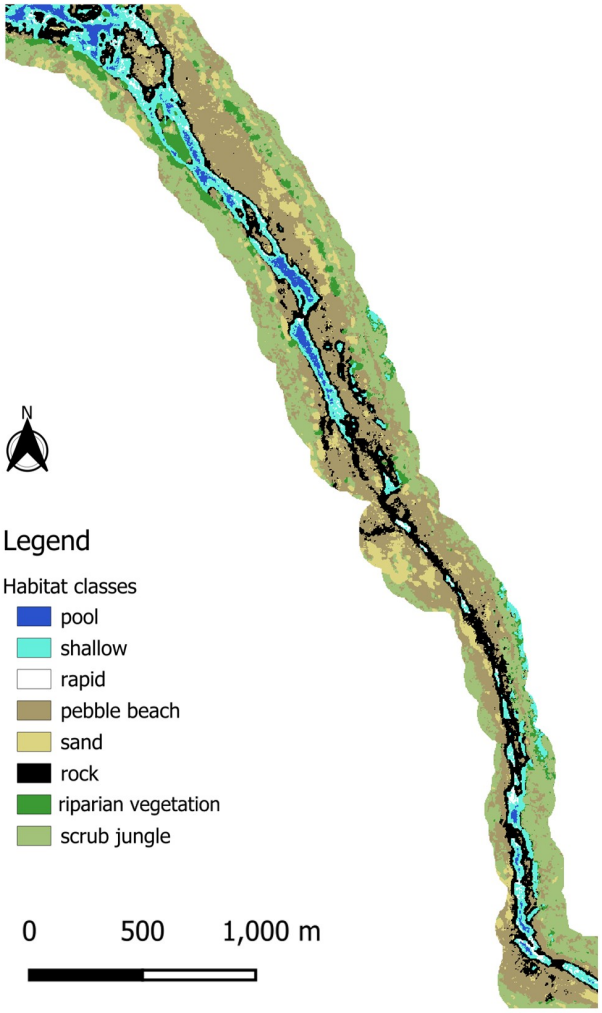

Figure 3.19. Habitat map generated by model T in Mekedatu.

Misclassified areas were found in the hills surrounding the river channel, compared to validation points (**Figure 3.20**). The area corresponds in reality to scrub jungle, and was classified as a mix of shallow, rock, pebble beach and scrub jungle.

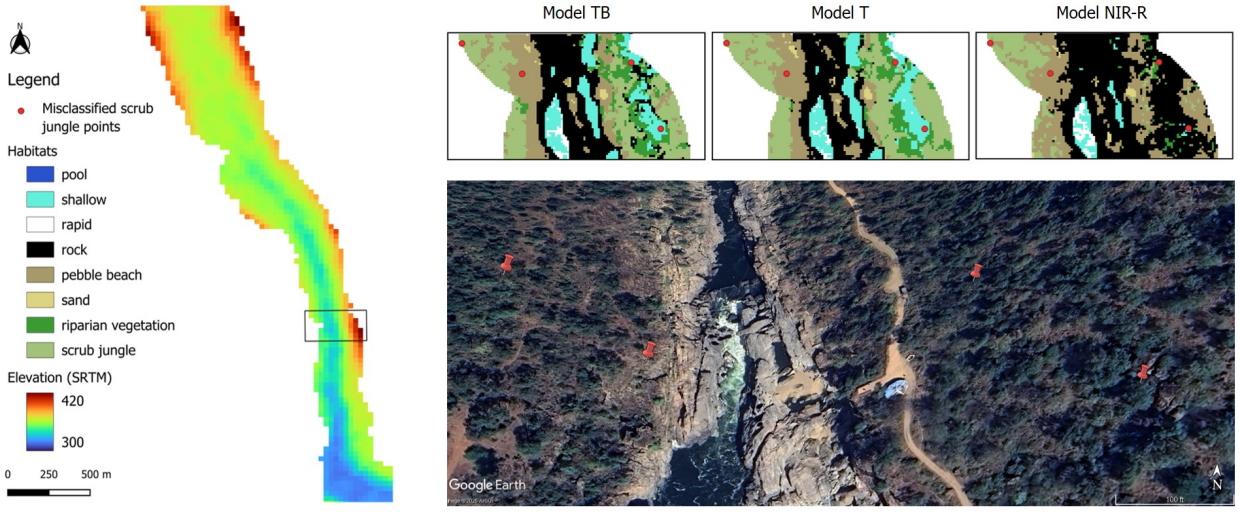

Figure 3.20. Misclassified scrub jungle points in Mekedatu, in relation to terrain elevation. The results for each model are compared to Airbus imagery.

Chapter 4

Discussion

This study integrated local knowledge, UAV, and PlanetScope imagery into automatic and scalable Humpback Mahseer habitat mapping. While earlier studies showed the potential of using supervised classification for riverine habitat mapping (Giroux et al., 2022, Zhang and Fryirs, 2024, Berhane et al., 2018), none of them addressed fish habitat classification on the meso-scale using high-resolution satellite imagery. This study showed that it is feasible to use UAV-derived training samples from local knowledge on high-resolution satellite imagery, despite the difference in image resolution.

To develop an automated habitat mapping method, this study investigated local knowledge integration in deriving training samples from UAV imagery, which predictors can be used in supervised classification, and which model produces the most scalable and accurate results.

4.1 Training data

Local knowledge was effectively used to create an initial set of samples, and to refine them iteratively, based on visual assessment of preliminary results and sample size adjustment. The training samples were derived in three iterations. The first two iterations showed classification noise on preliminary results. Implementing feedback from local experts and increasing the average sample size reduced classification noise in the third iteration. The sample sizes were proportional to the habitat types, but a minimum of 225m^2 was aimed for the average size of each class. Rapid was the only class which did not reach the target average area.

This study confirmed the hypothesis that local expert knowledge can be effectively integrated in deriving training samples from UAV data, as suggested by previous studies (Roelfsema et al., 2021, Lauer and Aswani, 2008, Xiong et al., 2017). This approach proved to be particularly useful in this study, where only one UAV image was available. It also supported the hypothesis that UAV-derived training samples can be used in Random Forest classification on PlanetScope data, despite of the resolution difference. The result improvement across iterations can be correlated with the increase in average training sample size. This supports the hypothesis that the size and quality of training samples influences results, as suggested by Millard and Richardson

(2015). The rapid class did not reach the minimum sample area, because rapids are naturally small and defining large enough samples was challenging (Sreenivasan and Mahesh, 2021).

Collecting training samples or validating the UAV-derived samples in the field would have likely provided more robust samples (Giroux et al., 2022, Wegscheider et al., 2020). Therefore, a limitation in training data creation related to the timing of the study. Organizing the field campaign in February 2025 was the earliest possible period in the time frame of the study. The study started in September 2024, during monsoon, when the entire river bed was inundated and data collection was not possible. Therefore, fieldwork was conducted in February, at the beginning of the dry season. During fieldwork several elements of river dynamics were observed and discussed. For example, rocks within the main river channel can become rapids when water level increases. Field observations showed rock areas covered in sand and pebble covered in dry moss, which looks like sand. Rocks within the river serve as seasonal rapids, sand-covered rock has the ecological function of rock, and moss-covered pebble has the ecological function of pebble. Although ecologically these areas can be associated with one of the main habitat types, from a supervised classification perspective, the distinct characteristics can pose challenges.

Further studies on Humpback Mahseer habitat classification should consider separating habitats into different subhabitats. Subhabitats can be defined as separate classes, and then merged into a single class by their main function. Further delimitation between *land rock* and *water rock* could improve habitat classification.

4.2 Predictors in habitat mapping

To evaluate predictor choice in habitat mapping, this study conducted the following analysis: predictor selection based on correlation and variance analysis of bands and textures, followed by variable importance in each model, and a comparison of classification results across models and areas.

Predictor selection

During literature review, remote sensing imagery and textural features were found to be relevant in habitat mapping. Upon analysis, the uncorrelated bands were red and near-infrared (NIR), and uncorrelated textures were homogeneity, entropy, and variance. The variance texture had the lowest explained variance (18%), while entropy had the highest (30%).

Although different predictor combinations have been explored by previous studies, none of them showed a comparative predictor analysis on fish habitat classification, focusing on model generalization. While Giroux et al. (2022) used textures for salmon habitats, the study was performed on small-scale UAV transects. In their study, Berhane et al., 2018 compared different predictors, but in the context of wetland mapping, which differs from fish habitat mapping. Including texture features as predictors is supported by previous similar studies (Giroux et al., 2022, Berhane et al., 2018, Zhang and Fryirs, 2024). Apart from textures, Berhane et al. (2018) used a multitude of predictor combinations to assess the optimal predictor choice

for wetland mapping. Predictors included hydrogeomorphology variables, elevation data, and spectral indices related to vegetation, soil, and water. In their study, Zhang and Fryirs (2024) used high-resolution elevation data dervied from LiDAR, satellite bands, and textures to map geomorphic units within river channels, which are similar to fish habitats in terms of scale and context.

The correlation analysis was performed only on the Galibore extent within the PlanetScope image. This creates a limitation, as correlation analysis only on the training area might not have been representative for the test areas as well, or for future study areas. Morever, texture feature correlation was only analysed on the NIR band, starting from the assumption that since it is the most uncorrelated with highest variance, it would be the most representative. However, applying correlation and variance analysis on all textures on all bands might have led to different results. The choice was based on practical considerations, because creating texture features is computationally expensive.

Further research should consider larger areas for correlation analysis, as relationships between bands might be different in the training area than over the entire study area. Moreover, further analysis could be done in assessing the correlation of all textures computed on all bands, instead of only on the NIR band. With sufficient time and financial resources, additional variables, such as spectral indices, elevation data and hydrogeomorphological variables could be explored. For example, the normalized vegetation difference index (NDVI), the normalized difference soil index (NDSI), and the normalized difference water index (NDWI) could be analyzed, as suggested by Berhane et al. (2018). Moreover, local spatial statistics such as Local Moran's I, Getis-Ord Local Gi and Local Geary's C could be explored, as suggested by Collin et al. (2011).

Variable importance

In this study, three Random Forest models were trained on different predictor choices. The first model (denoted TB) included all PlanetScope bands (blue, green, red, NIR), and the uncorrelated textures (homogeneity, entropy, variance) computed on all bands. The second model (denoted T) included only the uncorrelated textures computed on all PlanetScope bands. The third model (denoted NIR-R) included the red and NIR bands, and the uncorrelated textures computed on the red and NIR bands. The highest variable importance was the variance of the red band in all models, followed by the variance of the NIR band. The highest values of these predictors were in model T, when compared to the other models. In all models, homogeneity and entropy features had the least importance.

Variance is a measure of spread of intensity values (Hall-Beyer, 2017). Therefore, it helps in differentiating habitats with varying levels of heterogeneity. Entropy is a measure of randomness. Even though the habitats have high heterogeneity, they tend to have structured patterns within the classes, which decreases the relevance of entropy. Homogeneity is a measure of closeness between neighbouring pixels, which makes it relevant in identifying more uniform habitats, such as pools, but less relevant in identifying habitats such as rapids. Moreover, the explained variance for the red and NIR bands was the highest, which most likely made the textures com-

puted on these bands more relevant compared to the blue and green bands.

A limitation that could have influenced variable importance is related to predictor choice. In the correlation analysis, entropy had the highest variance, while the variance texture had the lowest explained variance among the textures. Nevertheless, variance had the highest importance in classification for all models. This shows that when correlated to the habitats, predictors can have high importance even though they show less variance. Therefore, even though some predictors have low variance, they still might be useful predictors.

Further studies should include a wider variety of predictors. Furthermore, variable importance could be analyzed on a preliminary model, and based on that, predictors could be chosen, instead of by correlation analysis. This could potentially improve the model, as predictors would be selected in relation to individual performance within the model.

Model comparison across areas

The models showed high similarities with each other in all areas, particularly Galibore (79%) and Bheemeshwari (76%). Mekedatu showed the lowest similarity between models (66%). Models T and TB are the most similar for all areas, whereas model NIR-R consistently classified pixels differently. Based on class confusion statistics between models, model TB showed preference for classifying pebble beach instead of scrub jungle in Galibore and Mekedatu, and shallow water instead of pools in Bheemeshwari. Model T showed a preference for shallow water in Bheemeshwari, and a preference for scrub jungle in Mekedatu. Model NIR-R showed a preference for classifying scrub jungle in Galibore and Mekedatu, and pools in Bheemeshwari.

The high similarity between models in Galibore might be due to overfitting, as Galibore was the training area. Bheemeshwari still had high similarity between models. Even though Bheemeshwari has a wider river channel and different landscape characteristics, it is still comparable to Galibore in terms of landscape. However, Mekedatu is a particular area, with a canyon-like structure, narrower river, and steeper hills. The different landscape can be a reason for the lower result similarity, which shows that model generalization decreases as landscape conditions change. The fact that model NIR-R consistently classified pixels differently is also visible in the compact and clustered spatial patterns of the model disagreement area where NIR-R classified pixels differently than TB and T.

The preference of the NIR-R model for classifying scrub jungle in Galibore instead of pebble beach can be attributed to the fact that within pebble beaches, there can be varying amounts of shrub. The red band is more sensitive to chlorophyll, while the NIR band is more sensitive to canopy structure (**Kodani et al., 2002**). This combination is likely to have made the model capture and overestimate the shrub within the pebble beach.

In Bheemeshwari, results showed preference towards shallows in models T and TB, and towards pools in model NIR-R. The shallow water is characterised by a green colour, which originates from the micro-vegetation and moss growing on the bottom of the shallow habitats. The red

band is particularly sensitive to chlorophyll (Kodani et al., 2002), therefore it can separate between the shallow water, where chlorophyll is visible, and the deep water, where it is not.

The model comparison per area reiterates the limitations posed by training sample creation, predictor choice and model training. However, it also provides insights into how predictors relate to specific habitat characteristics, having implications on future predictor choice. This can be done by qualitatively assessing how the predictors correlate to the studied habitats prior to including them into analysis.

4.3 Accuracy assessment

On average, model T was found to have the highest performance. Galibore had the highest accuracy metrics in all models, while Mekedatu had the lowest. Per area and class, results show that model T tends to classify individual habitats better in Galibore and Bheemeshwari, with a few exceptions. In Mekedatu, model TB outperformed the other models in the majority of habitats. However, model TB showed 0 recall and precision in classifying rapids, which is not the case in results of models T and NIR-R. In Galibore, certain rock points were classified as rapids or pebble beach. In Mekedatu, certain scrub jungle points were classified as pebble beach or shallows.

Results support the hypothesis that model T is likely more generalizable. In Mekedatu, the low scores, especially for rapid, can be attributed to poor rapid representation in the validation dataset. The validation points were labelled on Airbus imagery from 21.01.2022, which correspond to the end of the monsoon season, when water levels are higher. In March, water levels drop significantly. Therefore, it is likely that points which were annotated as rapids in the January imagery, became exposed rocks by March (Sreenivasan, 2025b). Due to river dynamics, rocks can become rapids when water levels increase (Sreenivasan, 2025b). Another misclassification in Galibore is a rocky area covered by sand, which is classified as pebble beach. This type of misclassification is likely due to the resolution difference between UAV (3cm) and PlanetScope (3m). Even though the UAV shows the area as a mix of rock and sand, the size of the rocks is likely too small to be captured by a model trained on coarser resolution.

Models were only trained on different combinations of bands and textures, which could pose a limitation. However, using only bands and textures proved to be feasible for this case study, providing relatively high accuracy scores for all areas, especially when using only textures. Although model TB provided higher accuracy scores in some habitats, model T showed more balanced metrics. Choosing model T in habitat mapping is likely to produce more balanced results for all classes than models TB and NIR-R. In Mekedatu, even though a large number of the individual habitats scored better in the TB model results, the metrics are more polarized than in the other models. Therefore, even though model T has lower scores on average, it is arguably preferable, as it tends to classify all habitats in a fairly representative way. This has important implications on future Humpback Mahseer habitat mapping. Using only textures computed on high-resolution satellite imagery bands is more cost-efficient and generalizable in data-limited environments than including additional datasets.

As a limitation, it is important to mention that validation was not fully independent. The initial strategy was to collect GPS points in the field. However, due to legislation issues regarding GPS use in India, a new strategy was developed after the results were obtained. However, by the time the validation strategy was reframed, all members of the research team had already seen the results. Therefore, an external team annotated the points to avoid bias. Arguably, the validation metrics would have been more representative if the points would have been annotated by experts within the research team. Moreover, the study did not integrate temporal river dynamics in the accuracy assessment. Another caveat is related to low accuracy scores in the hilly areas, visible especially in Mekedatu.

Further studies should investigate more independent validation methods. A suggested approach is point labelling by ecology experts on high-resolution imagery, with additional field validation of those points (**Fallati et al., 2020**, **Cho et al., 2014**, **Pulighe et al., 2016**). Another approach would be directly measuring GPS points in the field. However, Indian legislation on satellite communication use needs to be considered. In addition, to formally include temporal dynamics and ecological expert knowledge in the accuracy assessment, rules could be derived from local ecology experts and integrated into post-processing to improve accuracy. Elevation data could be included in post-processing, to improve classification in misclassified hilly scrub jungle areas.

Chapter 5

Conclusions

This study aimed to integrate local knowledge, UAV and PlanetScope imagery into an automatic and scalable method for mapping Humpback Mahseer habitats in the Cauvery River.

Overall, results showed that PlanetScope imagery and textural features can be successfully combined with UAV-derived training samples from local knowledge in supervised classification of Humpback Mahseer habitats in the Cauvery River. Using local knowledge proved effective in creating training samples, and an iterative approach involving local experts improved their quality. Using only textural features in model training proved to be the most accurate and scalable.

All findings support further classification for other river stretches in the Cauvery River. Given that habitat degradation in the Cauvery River represents the biggest threat to the survival of Humpback Mahseers, this study provides actionable data and methods to derive river habitat maps to support conservation efforts. This research provides the Wildlife Association of South India with a method to determine areas that need protection. When river stretches are declared protected areas, they are less vulnerable to threats such as damming, water extraction, deforestation, and unethical fishing practices. Habitat maps help justify this need to government agencies.

Although this study showed promising results, it still faces several limitations. Creating the training samples relied on UAV-derived data, instead of in-field measurements. The monsoon season, which coincided with the beginning of the study, limited a more robust and independent data collection strategy. Creating the validation data was affected by the same limitations. Regarding model comparison, only three predictor combinations were evaluated, which limited a more complex predictor analysis.

Future work should focus on combining habitat maps with fish movement data to extract habitat preferences and population trends for Humpback Mahseers. Habitat trends would indicate favourable habitat traits for Humpback Mahseers, and maps would locate areas that meet these conditions. Future studies should focus on building a multi-temporal PlanetScope collection for the Cauvery River. This would enable the method to be applied on different river scales, revealing larger-scale habitat composition patterns for area-specific conservation strategies. Regarding model improvement, scalability should be tested on larger areas, contextual classification can be considered to improve class separation, and more predictors can be evaluated.

Bibliography

An, N. V., Quang, N. H., Son, T. P. H., and An, T. T. (2023). High-resolution benthic habitat mapping from machine learning on planetscope imagery and icesat-2 data. *Geocarto International*, 38(1).

Belletti, B., Rinaldi, M., Bussettini, M., Comiti, F., Gurnell, A. M., Mao, L., Nardi, L., and Vezza, P. (2017). Characterising physical habitats and fluvial hydromorphology: A new system for the survey and classification of river geomorphic units. *Geomorphology*, 283:143–157.

Berhane, T. M., Lane, C. R., Wu, Q., Autrey, B. C., Anenkhonov, O. A., Chepinoga, V. V., and Liu, H. (2018). Decision-tree, rule-based, and random forest classification of high-resolution multispectral imagery for wetland mapping and inventory. *Remote Sensing*, 10(4).

Blaschke, T. (2010). Object based image analysis for remote sensing. *ISPRS journal of photogrammetry and remote sensing*, 65(1):2–16.

Breiman, L. (2001). Random forests. *Machine learning*, 45:5–32.

Cauvery Neeravari Nigam Limited (2024). Pre-feasibility report of mekedatu balancing reservoir and drinking water project. Technical report, Cauvery Neeravari Nigam Limited, Mysore, India. Submitted to the Ministry of Environment, Forests and Climate Change (MOEF), Government of India.

Cho, H. J., Ogashawara, I., Mishra, D., White, J., Kamerosky, A., Morris, L., Clarke, C., Simpson, A., and Banisakher, D. (2014). Evaluating hyperspectral imager for the coastal ocean (hico) data for seagrass mapping in indian river lagoon, fl. *GIScience & Remote Sensing*, 51(2):120–138.

Collin, A., Long, B., and Archambault, P. (2011). Benthic classifications using bathymetric lidar waveforms and integration of local spatial statistics and textural features. *Journal of Coastal Research*, (62):86–98.

Fallati, L., Saponari, L., Savini, A., Marchese, F., Corselli, C., and Galli, P. (2020). Multi-temporal uav data and object-based image analysis (obia) for estimation of substrate changes in a post-bleaching scenario on a maldivian reef. *Remote Sensing*, 12(13).

Frazier, A. E. and Hemingway, B. L. (2021). A technical review of planet smallsat data: Practical considerations for processing and using planetscope imagery. *Remote Sensing*, 13(19).

Giroux, C., Grant, J., Brown, C. J., and Barrell, J. (2022). Remote sensing of river habitat for salmon restoration. *Frontiers in Remote Sensing*, 3:993575.

Gupta, N. (2015). *River Conservation in the Indian Himalayan Region*. PhD thesis, King's College, London.

Halder, T., Chakraborty, D., Pal, R., Sarkar, S., Mukhopadhyay, S., Roy, N., and Karforma, S. (2024). A hybrid approach for water body identification from satellite images using ndwi mapping and histogram of gradients. *Innovations in Systems and Software Engineering*, 20(2):111–120.

Hall-Beyer, M. (2017). Practical guidelines for choosing glcm textures to use in landscape classification tasks over a range of moderate spatial scales. *International Journal of Remote Sensing*, 38:1312 – 1338.

Hamilton, F. (1822). *An account of the fishes found in the river Ganges and its branches*, volume 1. Archibald Constable.

Hemalatha, S. and Anouncia, S. (2018). G-l fractional differential operator modified using auto-correlation function: Texture enhancement in images. *Ain Shams Engineering Journal*, 9(4):1689–1704.

Hurbean, L., Danaiata, D., Militaru, F., Dodea, A.-M., and Negovan, A.-M. (2021). Open Data Based Machine Learning Applications in Smart Cities: A Systematic Literature Review. *Electronics*, 10(23).

Ierodiaconou, D., Schimel, A. C., Kennedy, D., Monk, J., Gaylard, G., Young, M., Diesing, M., and Rattray, A. (2018). Combining pixel and object based image analysis of ultra-high resolution multibeam bathymetry and backscatter for habitat mapping in shallow marine waters. *Marine Geophysical Research*, 39:271–288.

IUCN (2024). Humpback Mahseer. https://www.iucnredlist.org/. Accessed: 2024-09-17.

Janowski, and Wróblewski, R. (2024). Application and evaluation of the ai-powered segment anything model (sam) in seafloor mapping: A case study from puck lagoon, poland. *Remote Sensing*, 16(14).

Kodani, E., Awaya, Y., Tanaka, K., and Matsumura, N. (2002). Seasonal patterns of canopy structure, biochemistry and spectral reflectance in a broad-leaved deciduous fagus crenata canopy. *Forest Ecology and Management*, 167(1):233–249.

Kotsiantis, S. B., Zaharakis, I., Pintelas, P., et al. (2007). Supervised machine learning: A review of classification techniques. *Emerging artificial intelligence applications in computer engineering*, 160(1):3–24.

Lauer, M. and Aswani, S. (2008). Integrating indigenous ecological knowledge and multi-spectral image classification for marine habitat mapping in oceania. *Ocean & Coastal Management*, 51(6):495–504.

Liu, R. (2017). Compositing the minimum ndvi for modis data. *IEEE Transactions on Geoscience and Remote Sensing*, 55(3):1396–1406.

Martin, T. G., Burgman, M. A., Fidler, F., Kuhnert, P. M., Low-Choy, S., McBride, M., and Mengersen, K. (2012). Eliciting expert knowledge in conservation science. *Conservation Biology*, 26(1):29–38.

Menon, S. and Bawa, K. S. (1997). Applications of geographic information systems, remote-sensing, and a landscape ecology approach to biodiversity conservation in the western ghats. *Current science*, pages 134–145.

Millard, K. and Richardson, M. (2015). On the importance of training data sample selection in random forest image classification: A case study in peatland ecosystem mapping. *Remote. Sens.*, 7:8489–8515.

Mohamed, H., Nadaoka, K., and Nakamura, T. (2022). Automatic semantic segmentation of benthic habitats using images from towed underwater camera in a complex shallow water environment. *Remote. Sens.*, 14:1818.

Nautiyal, P. (2014). Review of the art and science of indian mahseer (game fish) from nineteenth to twentieth century: road to extinction or conservation? *Proceedings of the National Academy of Sciences, India Section B: Biological Sciences*, 84:215–236.

Pagels, J., Chaouali, M., Fenwick, C., von Rummel, P., and Bebermeier, W. (2024). Coupling morphometric analysis and soil erosion modeling for the characterization of the geomorphological setting in the surrounding of the archaeological site of chimtou (central medjerda valley, tunisia). *Journal of Maps*, 20(1).

Pathak, B. and Barooah, D. (2013). Texture analysis based on the gray-level co-occurrence matrix considering possible orientations. *International Journal of Advanced Research in Electrical, Electronics and Instrumentation Engineering*, 2(9):4206–4212.

Pichler, M. and Hartig, F. (2023). Machine learning and deep learning-a review for ecologists. *Methods in Ecology and Evolution*, 14(4):994–1016.

Pinder, A. C., Katwate, U., Dahanakur, N., and Harrison, A. (2018a). Tor remadevii. *The IUCN Red List of Threatened Species*, (2018-2).

Pinder, A. C., Manimekalan, A., Knight, J. M., Krishnankutty, P., Britton, J. R., Philip, S., Dahanukar, N., and Raghavan, R. (2018b). Resolving the taxonomic enigma of the iconic game fish, the hump-backed mahseer from the Western Ghats biodiversity hotspot, India. *PLoS One*, 13(6):e0199328.

Pinder, A. C., Raghavan, R., and Britton, J. R. (2015a). Efficacy of angler catch data as a population and conservation monitoring tool for the flagship mahseer fishes (tor spp.) of southern india. *Aquatic Conservation: Marine and Freshwater Ecosystems*, 25(6):829–838.

Pinder, A. C., Raghavan, R., and Britton, J. R. (2015b). The legendary hump-backed mahseer tor sp. of india's river cauvery: an endemic fish swimming towards extinction? *Endangered Species Research*, 28(1):11–17.

Pinder, A. C., Raghavan, R., and Britton, J. R. (2020). From scientific obscurity to conservation priority: Research on angler catch rates is the catalyst for saving the hump-backed mahseer Tor remadevii from extinction. *Aquatic Conservation: Marine and Freshwater Ecosystems*, 30(9):1809–1815.

Portales-Julia, E., Mateo-Garcia, G., Purcell, C., and Gomez-Chova, L. (2023). Global flood extent segmentation in optical satellite images. *Scientific Reports*, 13(1).

Pulighe, G., Baiocchi, V., and and, F. L. (2016). Horizontal accuracy assessment of very high resolution google earth images in the city of rome, italy. *International Journal of Digital Earth*, 9(4):342–362.

Roelfsema, C. M., Lyons, M., Murray, N., Kovacs, E. M., Kennedy, E., Markey, K., Borrego-Acevedo, R., Ordonez Alvarez, A., Say, C., Tudman, P., Roe, M., Wolff, J., Traganos, D., Asner, G. P., Bambic, B., Free, B., Fox, H. E., Lieb, Z., and Phinn, S. R. (2021). Workflow for the generation of expert-derived training and validation data: A view to global scale habitat mapping. *Frontiers in Marine Science*, 8.

Rouse Jr, J. W., Haas, R. H., Deering, D., Schell, J., and Harlan, J. C. (1974). Monitoring the vernal advancement and retrogradation (green wave effect) of natural vegetation. Technical report.

Ruzza, G., Guerriero, L., Grelle, G., Guadagno, F. M., and Revellino, P. (2019). Multi-method tracking of monsoon floods using sentinel-1 imagery. *Water*, 11(11).

Sreenivasan, N. (2024). Personal communication during interview.

Sreenivasan, N. (2025a). Webinar: Citizen Naturalist Course. Life in a River.

Sreenivasan, N. (2025b). Personal communication. Field discussion with the in-field expert.

Sreenivasan, N. and Mahesh, N. (2021). Riverine habitat gradients and stream complexity during moderate-flow conditions in the Cauvery Wildlife Sanctuary (CWLS), Karnataka. Unpublished manuscript.

Stone, A., Hickey, S., Radford, B., and Wakeford, M. (2024). Mapping emergent coral reefs: a comparison of pixel- and object-based methods. *Remote Sensing in Ecology and Conservation*.

Tan, Y. H. J., Tham, J. K. Q., Paul, A., Rana, U., Ang, H. P., Nguyen, N. T. H., Yee, A. T. K., Leong, I, B. P., Drummond, S., and Tun, K. P. P. (2023). Remote sensing mapping of the regeneration of coastal natural habitats in singapore: Implications for marine conservation in tropical cities. *Singapore Journal of Tropical Geography*, 44(1):130–148.

Tang, Y., Jing, L., Li, H., Liu, Q., Yan, Q., and Li, X. (2016). Bamboo classification using worldview-2 imagery of giant panda habitat in a large shaded area in wolong, sichuan province, china. *Sensors*, 16(11).

Venot, J.-P., Reddy, V. R., and Umapathy, D. (2010). Coping with drought in irrigated south india: Farmers' adjustments in nagarjuna sagar. *Agricultural Water Management*, 97(10):1434–1442.

Ventura, D., Bonifazi, A., Gravina, M. F., Belluscio, A., and Ardizzone, G. (2018). Mapping and classification of ecologically sensitive marine habitats using unmanned aerial vehicle (uav) imagery and object-based image analysis (obia). *Remote Sensing*, 10(9):1331.

Verbyla, D. L. and Litvaitis, J. A. (1989). Resampling methods for evaluating classification accuracy of wildlife habitat models. *Environmental Management*, 13:783–787.

Wahidin, N., Siregar, V. P., Nababan, B., Jaya, I., and Wouthuyzen, S. (2015). Object-based image analysis for coral reef benthic habitat mapping with several classification algorithms. *Procedia Environmental Sciences*, 24:222–227.

Wegscheider, B., Linnansaari, T., and Curry, A. (2020). Mesohabitat modelling in fish ecology: A global synthesis. *Fish and Fisheries*, 21(5):927–939.

Wegscheider, B., Linnansaari, T., Ndong, M., Haralampides, K., St-Hilaire, A., Schneider, M., and Curry, R. A. (2024). Fish habitat modelling in large rivers: combining expert opinion and hydrodynamic modelling to inform river management. *Journal of Ecohydraulics*, 9(1):68–86.

Wheaton, J. M., Fryirs, K. A., Brierley, G., Bangen, S. G., Bouwes, N., and O'Brien, G. (2015). Geomorphic mapping and taxonomy of fluvial landforms. *Geomorphology*, 248:273–295.

Woodget, A. S., Austrums, R., Maddock, I. P., and Habit, E. (2017). Drones and digital photogrammetry: from classifications to continuums for monitoring river habitat and hydromorphology. *Wiley Interdisciplinary Reviews: Water*, 4(4):e1222.

World Population Review (2024). Bangalore population 2024. Accessed: 2025-04-05.

Xia, G.-S., Wang, Z., Xiong, C., and Zhang, L. (2015). Accurate annotation of remote sensing images via active spectral clustering with little expert knowledge. *Remote Sensing*, 7(11):15014–15045.

Xiong, J., Thenkabail, P. S., Gumma, M. K., Teluguntla, P., Poehnelt, J., Congalton, R. G., Yadav, K., and Thau, D. (2017). Automated cropland mapping of continental africa using google earth engine cloud computing. *ISPRS journal of photogrammetry and remote sensing*, 126:225–244.

Xu, X., Xu, S., Jin, L., and Song, E. (2011). Characteristic analysis of otsu threshold and its applications. *Pattern Recognition Letters*, 32(7):956–961.

Zagajewski, B., Kluczek, M., Zdunek, K. B., and Holland, D. (2024). Sentinel-2 versus planetscope images for goldenrod invasive plant species mapping. *Remote Sensing*, 16(4).

Zhang, H., Li, Q., Liu, J., Shang, J., Du, X., Mcnairn, H., Champagne, C., Dong, T., and Liu, M. (2017). Image classification using rapideye data: Integration of spectral and textual features in a random forest classifier. *IEEE Journal of Selected Topics in Applied Earth Observations and Remote Sensing*, 10:5334–5349.

Zhang, N. and Fryirs, K. (2024). A hierarchical method and workflow for the semi-automated mapping of valley bottom geomorphic units using publicly available remote sensing datasets. *Earth Surface Processes and Landforms*, 49(11):3524–3540.

Zheng, G., Li, X., Zhou, L., Yang, J., Ren, L., Chen, P., Zhang, H., and Lou, X. (2018). Development of a gray-level co-occurrence matrix-based texture orientation estimation method and its application in sea surface wind direction retrieval from sar imagery. *IEEE Transactions on Geoscience and Remote Sensing*, 56:5244–5260.

Appendix A

Mekedatu dam

The Cauvery Wildlife Sanctuary (CWS) is one of the most diverse natural areas in India (Sreenivasan, 2025a). The upper part of the CWS is particularly important, with former angling camps in Galibore, Bheemeshwari, and Doddamakali, which are relevant to Humpback Mahseer populations. The Mekedatu Gorge is the narrowest point of the entire 800km river course, having a canyon structure. However, the area between Doddamakali and Mekedatu (Figure A.1) is proposed to be transformed into a dam for generating hydroelectric power and drinking water to supply the city of Bangalore (Cauvery Neeravari Nigam Limited, 2024).

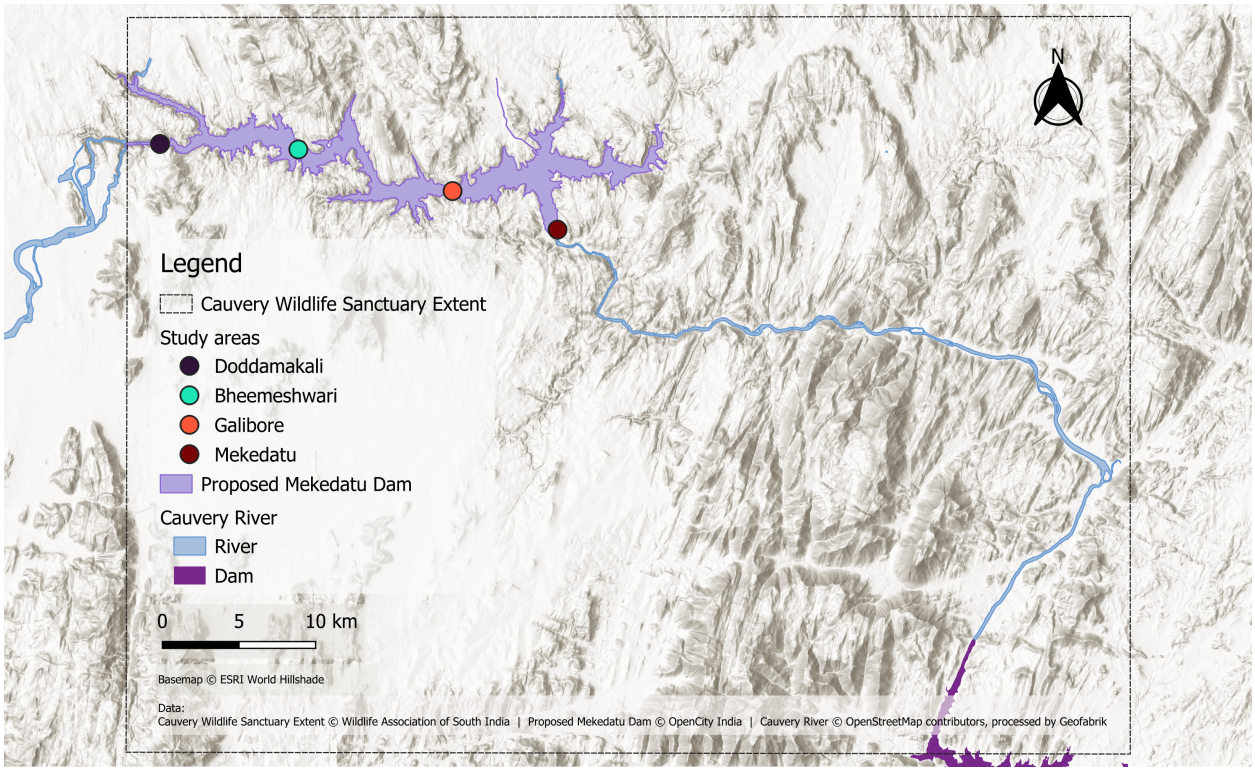

Figure A.1. Map of the proposed Mekedatu dam within the Cauvery Wildlife Sanctuary.

The claimed reason for building this dam is the water pressure that Bangalore and the surrounding areas are currently facing. With an ever increasing population of 14 million people only in the metropolitan area of Bangalore (World Population Review, 2024), the resource demands increase as well. The upstream Krishna Raja Sagara Dam already has a diversion that provides the needed water and energy supplies in the area.

However, the dam does not only supply water for Bangalore and the state of Karnataka. A quota of water needs to be released monthly to the state of Tamil Nadu. In the dry months, when water is scarce, the agreed quota is larger than the actual water reserves. Hence, Karnataka cannot provide the exact quota, but only a percentage. This creates social and political tensions between the states of Karnataka and Tamil Nadu, due to faulty definition of water obligations.

Mekedatu is a strategic point placed between the states of Karnataka and Tamil Nadu (Figure A.2). Building a dam around Mekedatu would allow Karnataka to store more water within the state, while still being able to deliver the quota to Tamil Nadu.

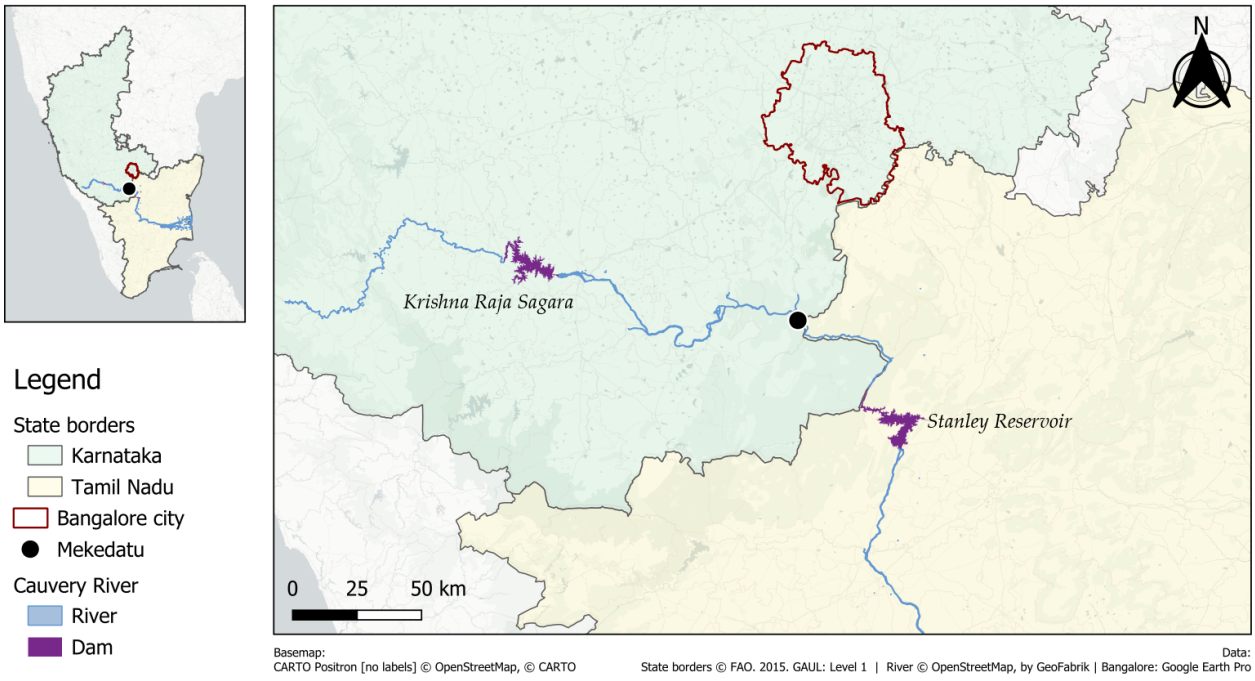

Figure A.2. Dams on the Cauvery River in Karnataka and Tamil Nadu.

Since almost the entire surface of the proposed dam is within the CWS, it does not meet the legal requirements for construction. However, a legal clause would allow the government to pump water directly from the river for drinking water. Using this clause would overlook the entire purpose of the initial project, which is also to generate hydroelectric power. Extracting drinking water from the CWS would be equally destructive for the riverine ecosystem. Habitat maps would support activism against the dam construction. With habitat heterogeneity proof, the Wildlife Association of South India would have actionable and data-driven evidence to present to governmental agencies.

Appendix B

Ecology of the riparian vegetation belt

The riparian vegetation belt is not only important to Humpback Mahseers, but to the entire ecosystem. The riparian belt represents an important food source for the herbivores living in the river valley, such as elephants, buffaloes (**Figure B.1a**), the grizzled giant squirrels (**Figure B.1b**), spotted and barking deer, and sambars (**Figure B.1c**).

(a) (b) (c)

Figure B.1. (a) Buffalo; (b) Grizzled giant squirrel; (c) Sambar.

However, the area is facing grazing pressure. An on-going study has shown presence of dicots in buffalo droppings, specific to the leaves of the trees from the riparian belt (**Sreenivasan, 2025b**). Buffaloes usually feed on grasses, which are monocots. Because of increasing population and more limited resources, buffaloes started grazing on saplings of the riparian belt trees. This prevents the riparian belt to develop, which in turn creates even more grazing pressure. This behaviour also indicates to imbalanced predator-prey relationships, which allow buffaloes to multiply uncontrollably. Moreover, this adds pressure on the entire ecosystem, as the vegetation belt is not developing any further. In time, if this trend continues, the riparian belt will not be strong enough to sustain the river bank and will lead to habitat and ultimately, ecosystem degradation.

Therefore, riparian vegetation needs to be considered in Humpback Mahseer conservation, even though it does not have a direct impact on the species.

Appendix C

Data management

Sharing and ownership

PlanetScope imagery is available through access from Wageningen University & Research, under the *Education and Research Basic* plan contract available from 2024-09-06 until 2026-09-06. PlanetScope data cannot be shared outside the scope of this research.

The UAV orthophoto belongs to the Wildlife Association of South India. The file cannot be used or shared outside the scope of this research.

C.1 Project data

A summary of the data used in the project is shown in Table C.1.

Table C.1. Source, process, and result data in the project.

Data stage	Data type	Software choice	Data size
Source data	PlanetScope image (multi-band raster)	QGIS, R	465MB
	PlanetScope UDM2 mask (multi-band raster)	QGIS, R	5.16MB
	PlanetScope metadata (XML file)	VSCode	10KB
	UAV orthophoto georeferenced (multi-band-raster)	QGIS	2.94GB
	Sentinel-1 VH data cube (multi-band raster)	Google Earth Engine, R, QGIS	181MB
Process data	Training samples - 3 iterations (geopackages)	QGIS, R	364KB
	Validation points - Galibore (geopackage)	QGIS, R	140KB
	Validation points Bheemeshwari & Mekedatu (KML, geopackage)	Google Earth Pro, R, QGIS	356KB
Result data	River boundaries for the study areas (geopackages)	R, QGIS	312KB
	Random Forest models (.RDS files)	R	1.81MB
	Random Forest predictions (single-band rasters)	R, QGIS	2.35MB
	Maps and figures (.jpg, .png files)	R, PowerPoint, Canva, Flourish	

C.2 Project structure

The project structure in R can be seen in Figure C.1.

```
.
└── thesis/
    ├── data/
    │   ├── extent/
    │   │   ├── bheemeshwari_extent.gpkg
    │   │   ├── galibore_extent.gpkg
    │   │   └── mekedatu_extent.gpkg
    │   ├── imagery/
    │   │   ├── planet/
    │   │   │   ├── 20240329_043235_57_24a7_3B_AnalyticMS_metadata.xml
    │   │   │   ├── 20240329_043235_57_24a7_3B_AnalyticMS_SR.tif
    │   │   │   └── 20240329_043235_57_24a7_3B_udm2.tif
    │   │   ├── radar/
    │   │   │   └── VH_Datacube_August_2024_Masked.tif
    │   │   └── uav/
    │   │       └── odm_orthophoto.tif
    │   ├── training/
    │   │   ├── first_iteration.gpkg
    │   │   ├── second_iteration.gpkg
    │   │   └── third_iteration.gpkg
    │   └── validation/
    │       ├── bheemeshwari_validation.gpkg
    │       ├── galibore_validation.gpkg
    │       └── mekedatu_validation.gpkg
    ├── results/
    │   ├── boundaries/
    │   │   ├── bheemeshwari_boundary.gpkg
    │   │   ├── galibore_boundary.gpkg
    │   │   └── mekedatu_boundary.gpkg
    │   ├── models/
    │   │   ├── model_it1.rds
    │   │   ├── model_it2.rds
    │   │   ├── model_it3.rds
    │   │   ├── model_nirr.rds
    │   │   ├── model_t.rds
    │   │   └── model_tb.rds
    │   └── predictions/
    │       ├── iterations/
    │       │   ├── galibore_predictions_iteration1.tif
    │       │   ├── galibore_predictions_iteration2.tif
    │       │   └── galibore_predictions_iteration3.tif
    │       ├── bheemeshwari_predictions_nirr.tif
    │       ├── bheemeshwari_predictions_t.tif
    │       ├── bheemeshwari_predictions_tb.tif
    │       ├── galibore_predictions_nirr.tif
    │       ├── galibore_predictions_t.tif
    │       ├── galibore_predictions_tb.tif
    │       ├── mekedatu_predictions_nirr.tif
    │       ├── mekedatu_predictions_t.tif
    │       └── mekedatu_predictions_tb.tif
    └── scripts/
        ├── data-preparation.R
        ├── functions.R
        ├── libraries.R
        ├── RQ1_iterations.R
        ├── RQ2_training.R
        └── RQ3_validation.R
```

Figure C.1. R project structure

C.3 Metadata

Table C.2 shows the metadata for the raster source data.

Table C.2. Raster files metadata.

General information	Title	UAV orthophoto (georeferenced)	PlanetScope image	Sentinel-1 VH Datacube
	Description	High-resolution UAV image capturing the area surrounding Galibore Nature Camp	High-resolution satellite image capturing the upper stretch of the middle course of the Cauvery River	Radar datacube, with all available imagery from August 2024 in the extent of the Cauvery Wildlife Sanctuary
	Author	Wildlife Association of South India	Planet Labs	European Space Agency, under Copernicus program
	Date	29.03.2024	29.03.2024	August 2024
Technical information	File format	TIF file (.tif)		
	Spatial resolution	3cm	3m	10m
	Radiometric resolution	32-bit Float	16-bit Integer	64-bit Float
	Colour space	Multi-spectral (RGB)	Multi-spectral (RGB-NIR)	-
	Sensor type	Optical sensor	PSB.SD	SAR
Geospatial information	Coordinate system	EPSG:32643		
	Units	Meters		
	Type	Projected		
	Method	Universal Transverse Mercator (UTM)		
	Accuracy	Based on World Geodetic System 1984 ensemble (EPSG:6326), which has a limited accuracy of at best 2 meters.		
	Reference	Dynamic (relies on a datum which is not plate-fixed)		
	Processing level	Level 3: ortho-rectified		

Appendix D

Validation points

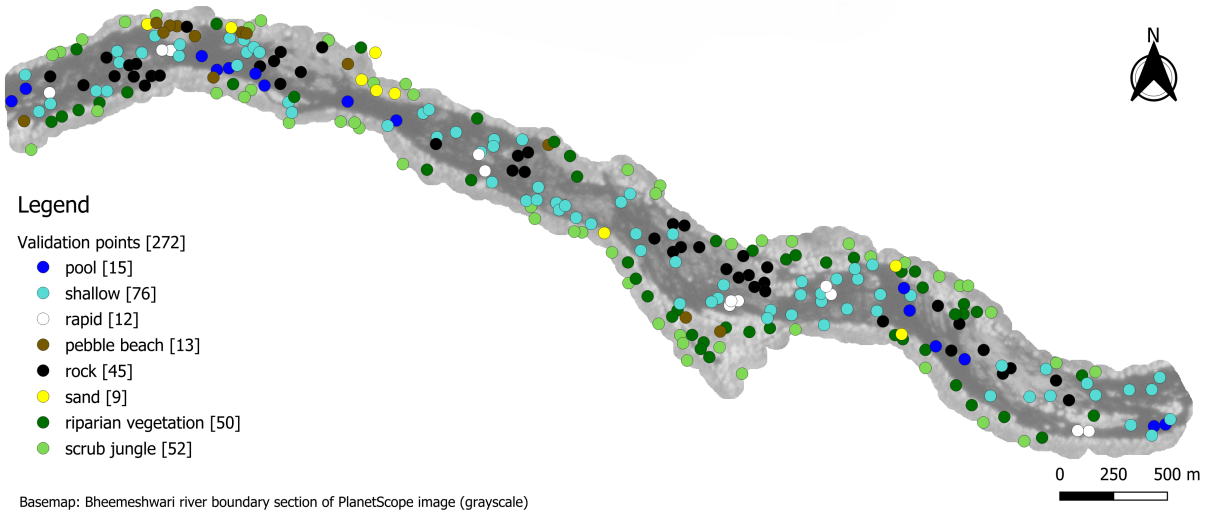

Figure D.1. Annotated validation points in Bheemeshwari.

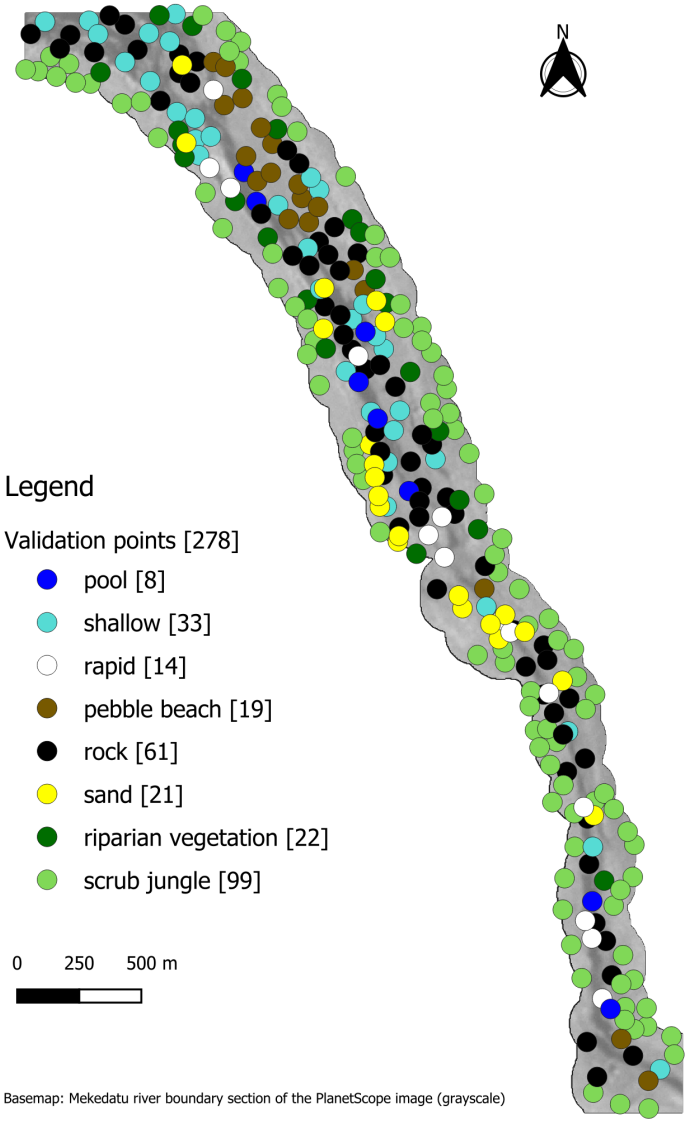

Figure D.2. Annotated validation points in Mekedatu.

Appendix E

Map comparison

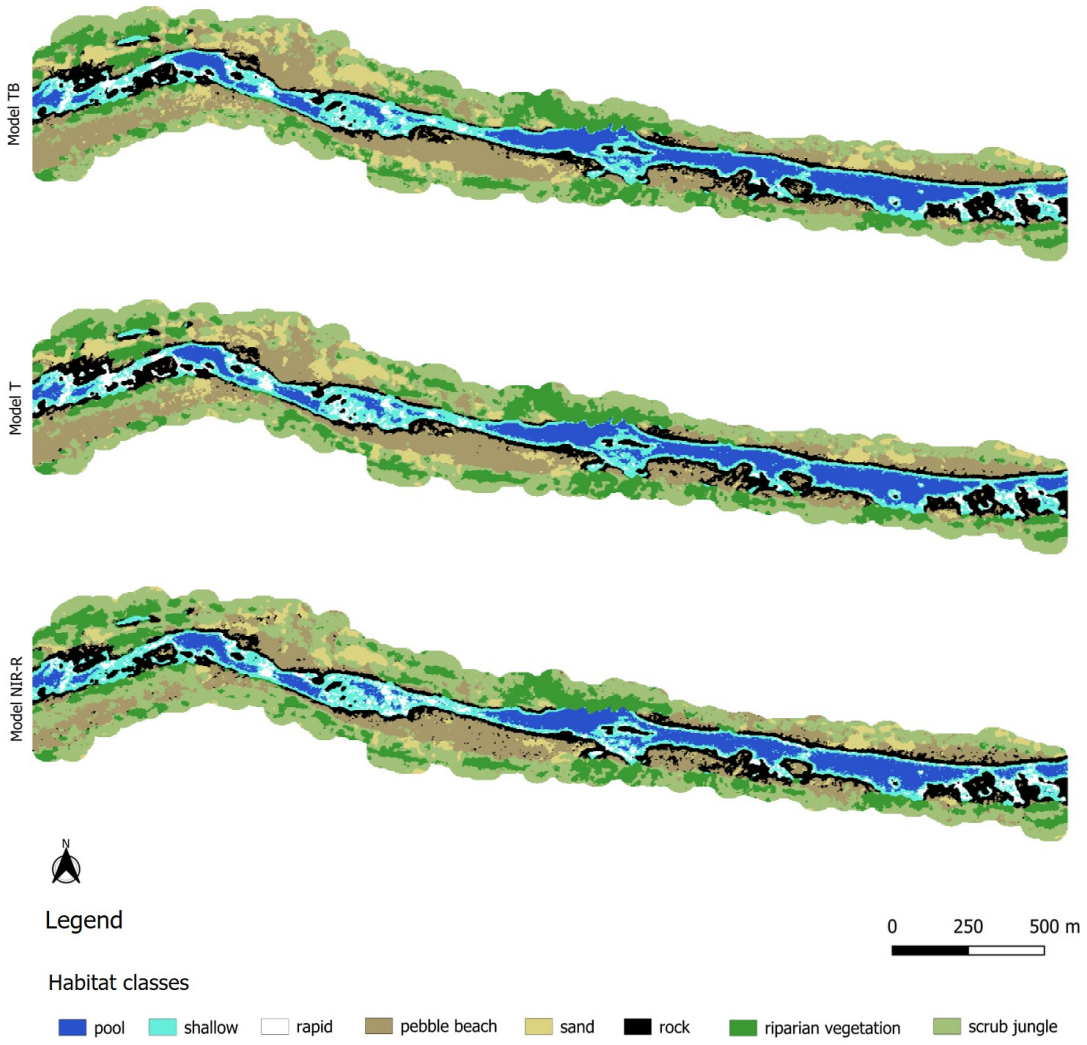

Figure E.1. Habitat maps in Galibore. Top to bottom: model T, model TB, model NIR-R.

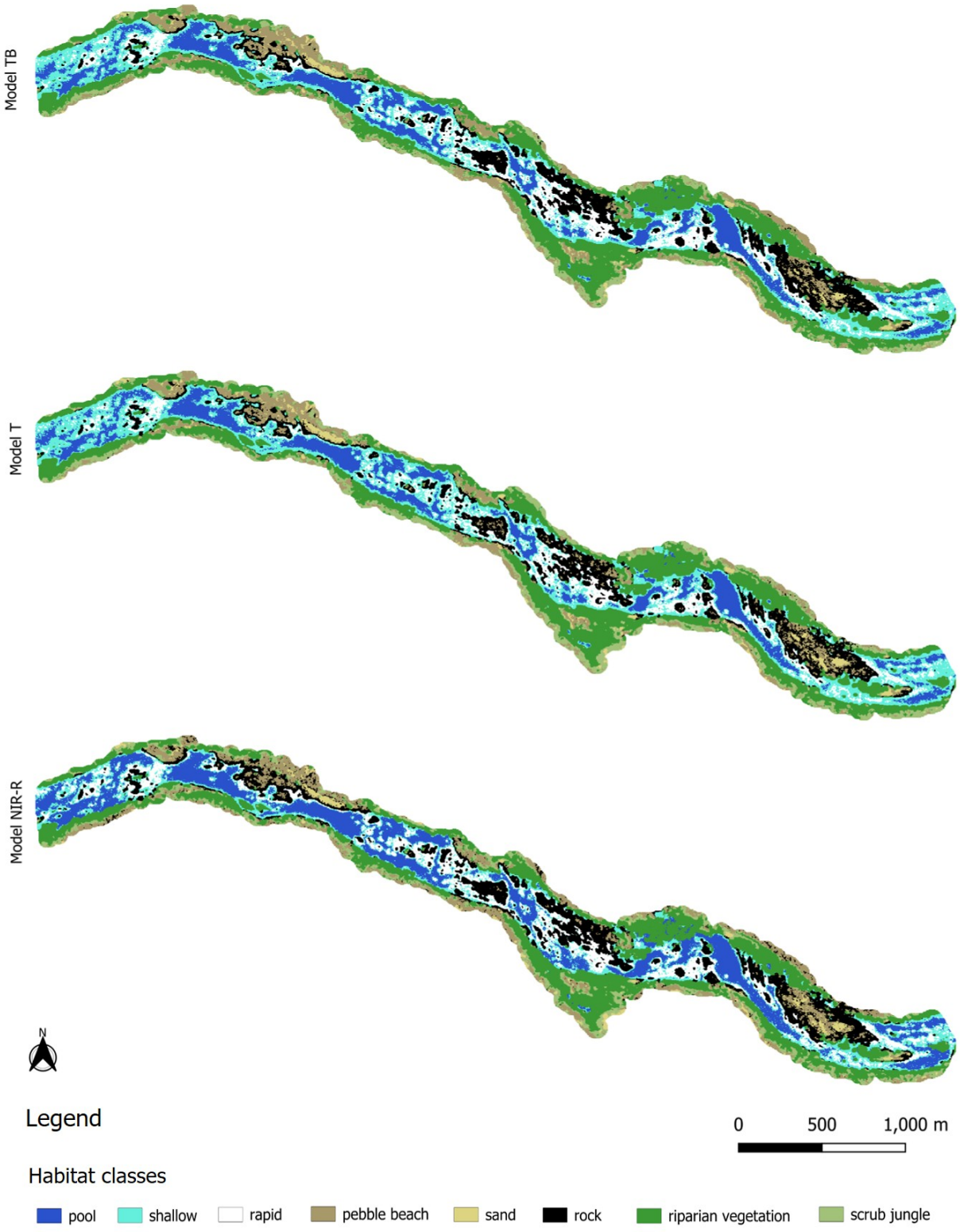

Figure E.2. Habitat maps in Bheemeshwari. Top to bottom: model T, model TB, model NIR-R.

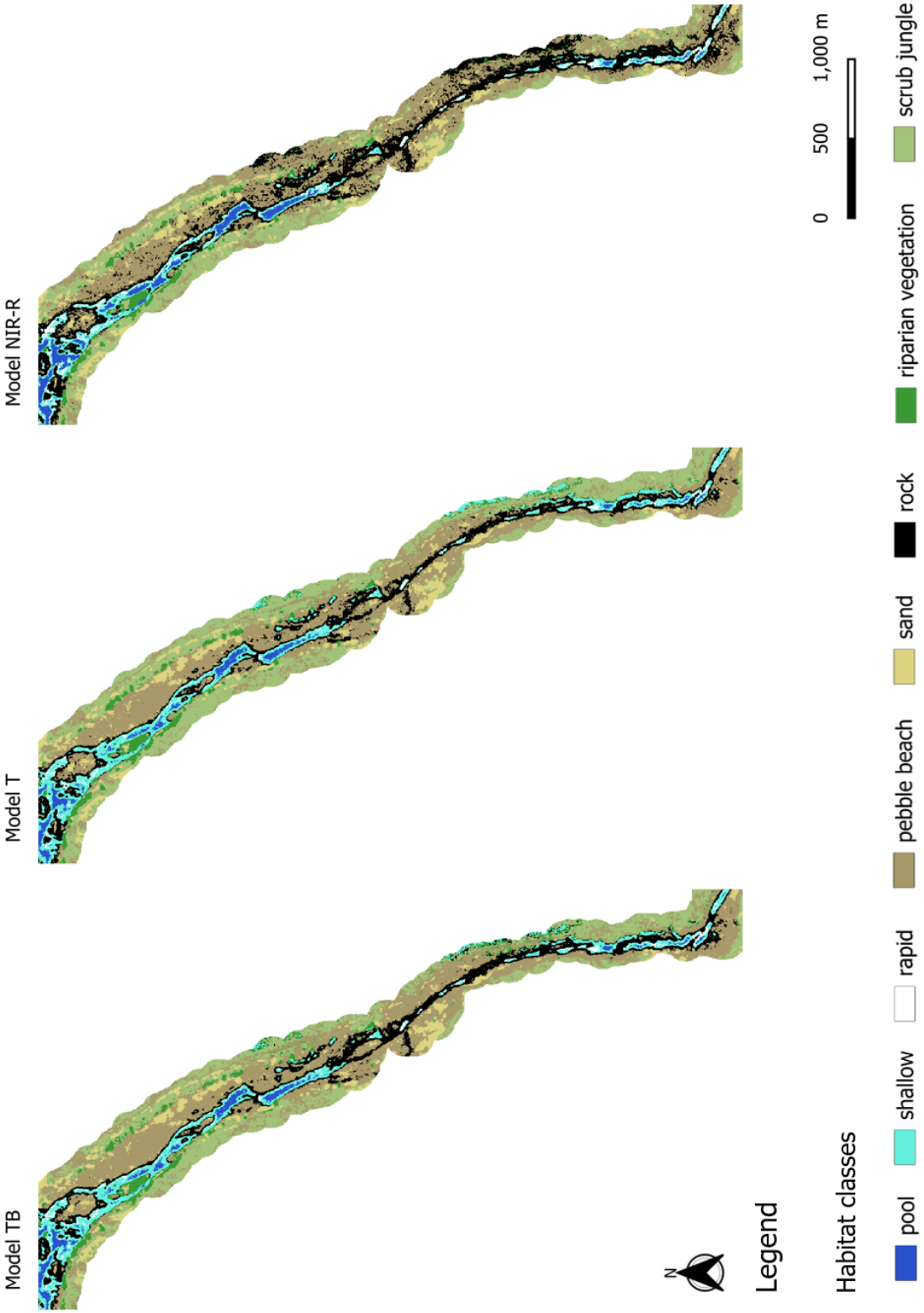

Figure E.3. Habitat maps in Mekedatu. Top to bottom: model T, model TB, model NIR-R.

Appendix F

Confusion matrices

The green-highlighted cells represent the true positive rate per class, i.e. the correctly classified pixels. The false positive rate per class is the sum per column, minus the true positive rate of the class. The false negative rate per class is the sum per row, minus the true positive rate of the class. The true negative rate per class is the sum of all cells, except for the row and the column corresponding to that class.

Galibore

Table F.1. Confusion matrix for the model trained on all bands and textures in Galibore.

		Predicted class							
		pebble beach	pool	rapid	rock	sand	scrub jungle	shallow	riparian vegetation
Real class	pebble beach	16	0	0	1	2	7	0	3
	pool	0	20	0	0	0	0	2	0
	rapid	0	0	9	0	0	0	11	0
	rock	12	0	2	8	2	2	2	0
	sand	7	0	0	2	6	3	0	0
	scrub jungle	4	0	0	0	1	36	0	6
	shallow	1	1	4	3	0	0	13	0
	riparian vegetation	0	0	0	0	0	6	0	17

Table F.2. Confusion matrix for the model trained only on textures in Galibore.

		Predicted class							
		pebble beach	pool	rapid	rock	sand	scrub jungle	shallow	riparian vegetation
Real class	pebble beach	14	0	0	1	3	10	0	1
	pool	0	21	1	0	0	0	0	0
	rapid	0	0	10	0	0	0	10	0
	rock	10	0	0	11	2	2	3	0
	sand	4	0	0	3	7	4	0	0
	scrub jungle	1	0	0	0	1	36	0	9
	shallow	0	1	3	4	0	0	14	0
	riparian vegetation	0	0	0	0	0	6	0	17

Table F.3. Confusion matrix for the model trained on red and near-infrared bands and textures in Galibore.

		Predicted class							
		pebble beach	pool	rapid	rock	sand	scrub jungle	shallow	riparian vegetation
Real class	pebble beach	10	0	0	1	0	17	0	1
	pool	0	19	1	0	0	0	2	0
	rapid	0	0	12	0	0	0	8	0
	rock	9	0	2	11	2	2	2	0
	sand	1	0	0	4	4	9	0	0
	scrub jungle	2	0	0	0	1	35	0	9
	shallow	0	1	7	5	0	0	9	0
	riparian vegetation	0	0	0	0	0	6	0	17

Bheemeshwari

Table F.4. Confusion matrix for the model trained on bands and textures in Bheemeshwari.

		Predicted class							
		pebble beach	pool	rapid	rock	sand	scrub jungle	shallow	riparian vegetation
Real class	pebble beach	9	0	0	1	0	0	0	3
	pool	0	11	0	0	0	0	4	0
	rapid	0	1	6	4	0	0	1	0
	rock	4	0	5	23	2	1	8	2
	sand	3	0	0	0	5	0	0	0
	scrub jungle	13	0	0	1	0	19	0	15
	shallow	1	14	20	5	0	0	33	3
	riparian vegetation	1	0	0	0	0	0	2	47

Table F.5. Confusion matrix for the model trained only on textures in Bheemeshwari.

		Predicted class							
		pebble beach	pool	rapid	rock	sand	scrub jungle	shallow	riparian vegetation
Real class	pebble beach	7	0	0	1	2	1	0	2
	pool	0	11	0	0	0	0	4	0
	rapid	0	1	6	4	0	0	1	0
	rock	4	0	2	23	2	1	11	2
	sand	3	0	0	0	5	0	0	0
	scrub jungle	13	0	0	1	0	18	0	16
	shallow	1	14	13	6	0	0	40	2
	riparian vegetation	0	0	0	0	0	2	2	46

Table F.6. Confusion matrix for the model trained on red and near-infrared bands and textures in Bheemeshwari.

		Predicted class							
		pebble beach	pool	rapid	rock	sand	scrub jungle	shallow	riparian vegetation
Real class	pebble beach	5	0	0	1	0	5	0	2
	pool	0	14	0	0	0	0	1	0
	rapid	0	1	7	4	0	0	0	0
	rock	3	2	3	25	3	1	6	2
	sand	0	0	0	2	6	0	0	0
	scrub jungle	16	0	0	2	1	15	0	14
	shallow	0	29	17	6	0	1	21	2
	riparian vegetation	0	0	0	0	0	2	2	46

Mekedatu

Table F.7. Confusion matrix for the model trained on bands and textures in Mekedatu

		Predicted class							
		pebble beach	pool	rapid	rock	sand	scrub jungle	shallow	riparian vegetation
Real class	pebble beach	16	0	0	2	1	0	0	0
	pool	0	5	0	0	0	0	3	0
	rapid	0	0	0	9	0	0	5	0
	rock	30	0	0	25	2	1	2	1
	sand	3	0	0	2	16	0	0	0
	scrub jungle	33	0	0	1	4	58	1	2
	shallow	6	3	2	11	0	0	11	0
	riparian vegetation	2	0	0	0	2	12	0	6

Table F.8. Confusion matrix for the model trained only on textures in Mekedatu.

		Predicted class							
		pebble beach	pool	rapid	rock	sand	scrub jungle	shallow	riparian vegetation
Real class	pebble beach	14	0	0	1	4	0	0	0
	pool	0	5	1	0	0	0	2	0
	rapid	0	0	1	10	0	0	3	0
	rock	33	0	0	21	2	3	2	0
	sand	4	0	0	2	15	0	0	0
	scrub jungle	27	0	0	1	5	63	1	2
	shallow	7	4	2	10	0	0	9	1
	riparian vegetation	1	0	0	0	2	13	0	6

Table F.9. Confusion matrix for the model trained on the red and near-infrared bands and textures in Mekedatu.

		Predicted class							
		pebble beach	pool	rapid	rock	sand	scrub jungle	shallow	riparian vegetation
Real class	pebble beach	10	0	0	7	2	0	0	0
	pool	0	5	1	0	0	0	2	0
	rapid	0	0	1	9	0	0	4	0
	rock	28	0	0	26	4	1	1	1
	sand	2	0	0	2	16	1	0	0
	scrub jungle	40	0	0	10	7	41	0	1
	shallow	4	5	2	15	0	0	7	0
	riparian vegetation	4	0	0	0	1	12	0	5